REPUBLIC OF TURKEY

ADANA ALPARSLAN TÜRKEŞ SCIENCE AND TECHNOLOGY UNIVERSITY

GRADUATE SCHOOL OF NATURAL AND APPLIED SCIENCES

DEPARTMENT OF MECHANICAL ENGINEERING

ACTIVE PROTECTION OF ARMORED LAND VEHICLES USING WATER JET

HÜSEYİN AYDIN EKER

MASTER OF SCIENCE

ADANA 2022

REPUBLIC OF TURKEY
ADANA ALPARSLAN TÜRKEŞ SCIENCE AND TECHNOLOGY UNIVERSITY

GRADUATE SCHOOL OF NATURAL AND APPLIED SCIENCES
DEPARTMENT OF MECHANICAL ENGINEERING

ACTIVE PROTECTION OF ARMORED LAND VEHICLES USING WATER JET

HÜSEYİN AYDIN EKER
MASTER OF SCIENCE

SUPERVISOR
ASSOC. PROF. DR. MUSTAFA KILIÇ

ADANA 2022

I hereby declare that all information in this thesis has been obtained and presented in accordance with academic rules and ethical conduct. I also declare that, as required by these rules and conduct, I have fully cited and referenced all information that is not original to this work.

[Signature]

Hüseyin Aydın EKER

ABSTRACT

ACTIVE PROTECTION OF ARMORED LAND VEHICLES USING WATER JET

Hüseyin Aydın EKER
Department of Mechanical Engineering
Supervisor: Assoc. Prof. Dr. Mustafa KILIÇ
February 2022, 67 pages

Armored vehicles and tanks used in battlefield are faced with many threats and these threats are becoming more lethal every day due to the use of rapidly advancing weapons and chemical technologies. As a solution, strengthening armor has a negative effect on vehicle size/weight and maneuverability. For this reason, the methods of adapting the systems defined as active protection sysems to armored vehicles are currently being studied. These active protection systems eliminate the threat by detecting and destroying or by providing a missed target. In this thesis, the effect of different parameters of high pressure water jet, which can be used as an active protection system in armored vehicles, on anti-tank ammunition was investigated. In the study the effects of water jet velocity, spray nozzle diameter and spray/collision distance parameters on anti-tank ammunition were examined. In the study, numerical analysis of flow dynamics and mechanical effects on the material was made and ANSYS LS-Dyna Computational Fluid Dynamics programme was used.

For combinations of different nozzle diameters, water jet speed and collison distance resultant momentum and resultant impuls values are calculated. Determined values for nozzle diameters are 2-4-6 and 10 mm; water jet velocity 150 and 500 m/s; collision distance 200-300-400-600 and 1000 mm. A range between 0.017 and 0.798 kgm/s is observed for resultant momentum. Impuls range varied between 0.0088 and 11.3292 MPa.ms. It is thought that the results of this study will be useful in the development of new type of active protection systems in the fields of defense and weapons industry in the future.

Keywords: Active protection system, fluid/solid surface interaction, high pressure water jet, Computational fluid dynamics.

ÖZET

SU JETİ KULLANARAK ZIRHLI KARA ARAÇLARINA AKTİF KORUMA SAĞLANMASI

Hüseyin Aydın EKER
Makina Mühendisliği Anabilim Dalı
Danışman: Doç. Dr. Mustafa KILIÇ
Şubat 2022, 67 sayfa

Harp alanlarında kullanılan zırhlı araç ve tanklar pek çok tehdit ile karşı karşıya kalmaktadır. Bu tehditler hızla ilerleyen silah ve mühimmat teknolojilerinin kullanımı nedeniyle her geçen gün daha ölümcül hale gelmektedir. Çözüm olarak öngörülen zırhın arttırılması, araç boyut/ağırlık ve manevra kabiliyeti üzerinde olumsuz etkiye sahiptir. Bu nedenle günümüzde aktif koruma sistemi olarak tanımlanmış sistemlerin zırhlı araçlara adapte edilmesi yöntemleri üzerinde çalışılmaktadır. Aktif koruma sistemleri, yüksek hızlı tanksavar mühimmatını tespit edip, yok ederek veya hedef şaşmasını sağlayarak tehdidi bertaraf etmektedir. Bu tezde; zırhlı araçlarda aktif koruma sistemi olarak kullanılabilecek yüksek basınçlı su jetinin farklı parametrelerinin tanksavar mühimmatı üzerine etkisi araştırılmıştır. Çalışmada; su jeti hızı, püskürtme nozul çapı ve püskürtme/çarpışma uzaklıkları parametrelerinin tanksavar mühimmatı üzerindeki etkileri irdelenmiştir. Akış dinamiğinin ve malzeme üzerindeki mekanik etiklerin sayıal olarak incelenmesi yapılmış ve ANSYS LS-Dyna Hesaplamalı Akışkanlar Dinamiği programı kullanılmıştır. Farklı püskürtme nozul çapı, su jet hızı ve çarpışma mesafesi kombinasyonu için momentum ve sonuçta ortaya çıkan impuls değerleri simüle edilmiştir. Nozul çapları için belirlenen değerler 2-4-6 ve 10 mm'dir; su jeti hızı 150 ve 500 m/s; çarpışma mesafesi 200-300-400-600 ve 1000 mm olarak seçilmiştir. Momentum için 0.017 ile 0.798 kgm/s; impuls için 0.0088 ile 11.3292 MPa.ms değer aralığı belirlenmiştir.
Bu çalışma sonuçlarının gelecekte, savunma ve silah sanayi alanlarında yeni tip aktif koruma sistemlerin tasarımında ve üretiminde faydalı olacağı değerlendirilmiştir.

Anahtar Kelimeler: Aktif koruma sistemi, Akışkan/katı yüzey etkileşimi, Yüksek basınçlı su jeti, Hesaplamalı akışkanlar dinamiği.

To m[illegible]ily.

ACKNOWLEDGEMENTS

TABLE OF CONTENTS

LIST OF FIGURES

LIST OF TABLES

NOMENCLATURE

APS	: Active Protection System
MBT	: Main Battle Tank
g	: gram
C	: explosive charge
M	: explosive mass
WJ	: water jet
AWJ	: abrasive water jet
We	: Weber number
Re	: Reynolds number
SIJA	: Single Impact Jet Apparatus
MIJA	: Multi Mmpact Jet Apparatus
SBWJG	: Split Bar Water Generator
TNT	: Trinitrotoluene
l_c	: Water jet core length
RPG	: Rocket Propelled Grenade
ATGM	: Anti-Tank Guided Missile
p	: pressure
P	: Momentum
HEAT	: High Explosive Anti Tank
KE	: Kinetic Energy
c_0	: Speed of sound in water
ρ	: density
E_c	: Modulus of compressibility
μ	: Dynamic viscosity
W	: Explosive weight
Z	: Scaled distance
P_{so}	: Side of pressure
$C_{r\alpha}$	: Reflection coefficient
CFD	: Computational Fluid Dynamics
σ	: Surface tension of water
σ_y	: Flow stress

σ_{eff}	: Effective stress
ϵ	: Plastic strain
E_v	: Internal energy per volume
Υ_0	: Gruniesen gamma
D_p	: Damage parameter
AoC	: Angle of contact

1. INTRODUCTION

A chemical reaction of milliseconds that causes hot gas and energy release, with very high pressure and temperature, is called an explosion. Hot gases formed by explosion make wave-type propagation to cover the volume proceeding spherically through an unbounded surrounding medium. In air blasts, just like hot gases air also expands which results in overlaying the air molecules causing a blast wave.

The pressure value and the speed of shock wave propagation develop inversely with the distance from the center of the explosion.
Sudden expansion following the blast, creates a vacuum phase where suction forces occur and is followed by a fluctuation in pressure ending with equalizing with ambient pressure (Vasilis and Solomos, 2013). Phases of an explosion is given in Figure 1.1.

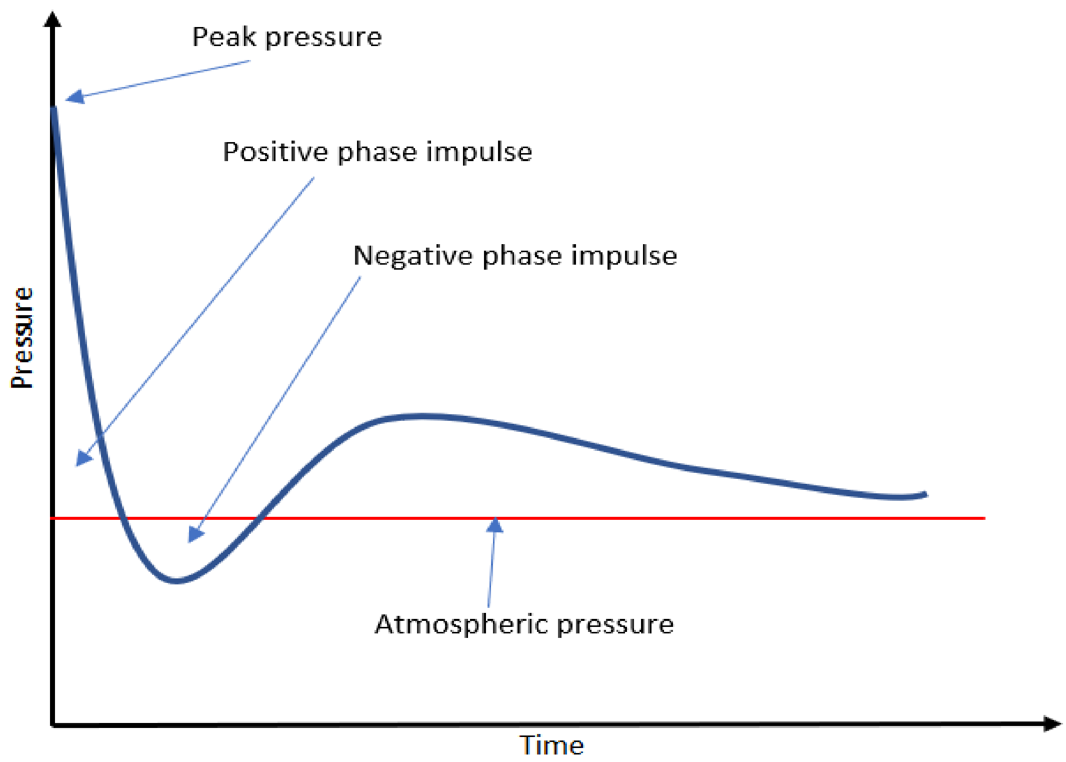

Figure 1.1. Typical pressure-time curve of a shock wave

A rocket is an unguided missile and a missile is a guided rocket causing explosion and damage at the point of contact. Armoured vehicles exposing an explosion in the field can experience vehicle damage and crew injury is highly probable. When the shock wave formed after the explosion contacts with the armored vehicle, the wave motion is transferred to the vehicle body. As a result of this interaction and transmission, primary and reflected shock waves are emitted within the armored vehicle. In Figure 1.2. pressure countours of an explosion is given. Serious injuries can occur to the human body exposed to the variable load caused by the phase difference of these shock waves and these injuries can result in death (Yang, Liou, Sheng, Gorsich, & Arepally, 2011).

Figure 1.2. Pressure countours of an explosion near an armoured vehicle (Tai et al., 2007)

Protecting vehicles using extra strong armour is an option but armored vehicles must react very quickly to tactical movements, so it is a priority for armored vehicles to have high mobility, so weight and maneuverability ratio is a limiting factor (Tai, Teng, Lo and Liu, 2007). Therefore a search for different methods was started to protect the vehicle.

Active Protection Systems are developed to detect, monitor and respond to a wide range of threats such as rocket-propelled grenades (RPGs) and anti-tank guided missiles (ATGMs). It can eliminate the threat by hard kill or soft kill operations. Simple representation of hard and soft kill is given in Figure 1.3. APS can be integrated into armored vehicles or the vehicle can be designed with APS.

Russian APS Arena’s working sequence is described briefly as followed. Radar scans for approaching threat within 50 meters in the designated speed band. When there is a threat to main battle tank (MBT) protection system is activated in 0.05 seconds and then operates automatically. It will not respond to false images or targets. In the target tracking mode radar locks the target 7.8 and 10.6 meters. Computer meanwhile analysis the data of the target and selects the appropriate countermunition. A small projectile is fired into the path of approaching target which is detonated 1.3-3.9 meters from the target. Detonation generates a field of destructive elemens destroying or disabling the target. System refreshes itself in 0.2-0.4 s to repel the new one (Meyer, 1998).

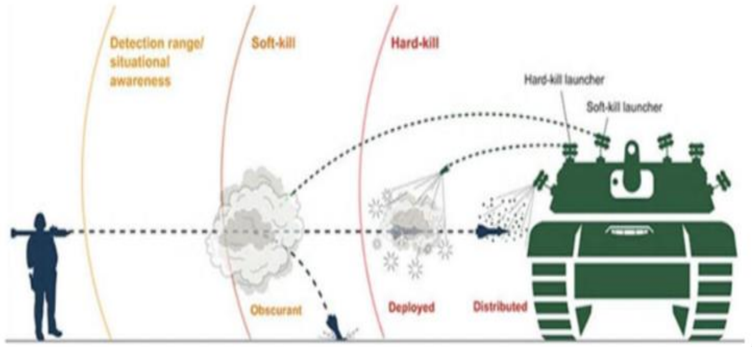

Figure 1.3. Hard and soft kill active protection system (Chant, 2013).

If APS is used, the requirement to strengthen the armor to protect the vehicle against threats is prevented. While designing a new armored vehicle, the armor requirement of the vehicle can be re-evaluated, resulting in a lighter and more agile war machine.

The aim of this study is evaluating high pressure water jet usage as a countermeasure attack against missiles like an active protection system and investigate its success.

1.1. Water Jets

In water jet technology, water or a mixture of water and abrasive material is accelerated at very high pressures. In this way, a wide range of materials can be mechanically eroded or simply cut. In Figure 1.4. abrasive water jet is described.

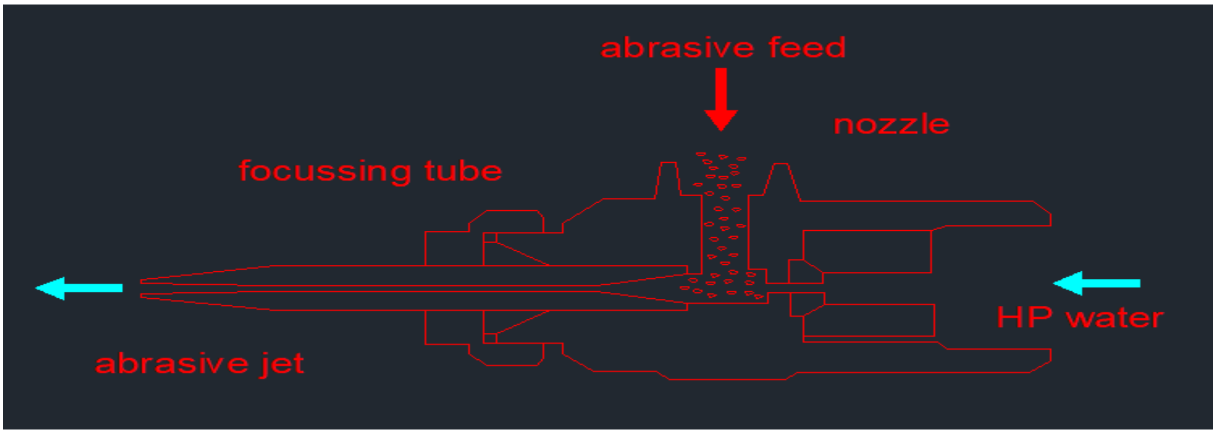

Figure 1.4. Abrasive water jet generation

Although many ancient civilizations, such as Egyptians and Romans, used the power of water in mining and agriculture, advanced use of pressurized water occurred in 19^{th} century during Californian gold rush to remove sand and mineral layers (Water Jet CuttingA Technology on the Rise). Effects of water jet on Darley Dale Sandstone is given in Figure 1.5.

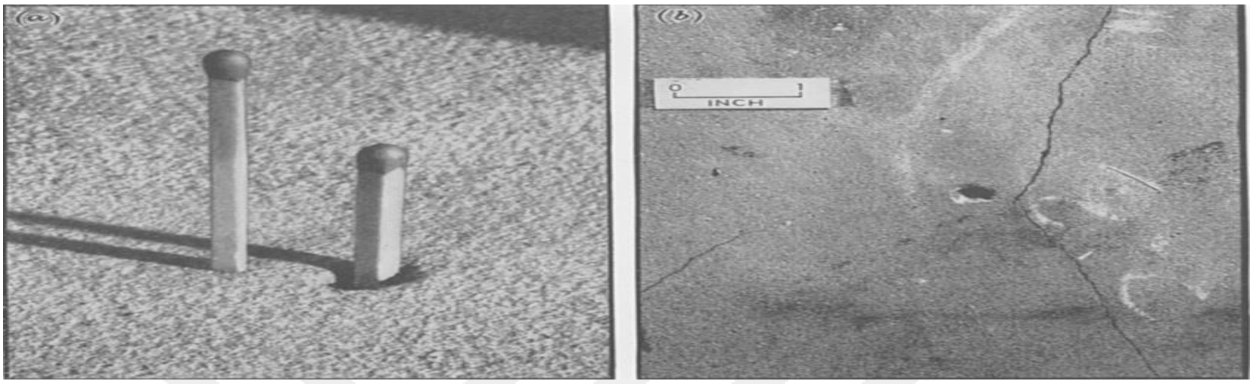

Figure 1.5. A shot of 10 cm3 water at 1000 m/s drills a 5mm hole with a depth of 20 mm at Darley Dale Sandstone which has a compressive strength of 67 MPa. Nozzle diameter: 1 mm – Distance: 25 mm (Leach et al., 1966).

Since 1920s water jets have been used for military purposes, such as discarding high explosive munitions. With pure water jet, many soft, sensitive, or hard materials can be cut mechanically precisely. Unfortunately, the same is not valid for very hard material handling with plain water jets. Invention of Abrasive Water Jets (AWJ) make it possible to cut hard materials such as steels, super alloys and ceramics (Miller, 2018).

The cutting process is based on giving energy to the material to break the chemical bonds between the atoms of the material. The energy of the fast-moving water jet or abrasive water jet is used to create micro erosion in the workpiece in the same manner.

1.1.1 Types of Commercial Water Jets

Commercial waterjets are given in three groups releated with abrasive mechanism of system.

1.1.1.1 Abrasive Water Jet

Abrasive is entrained into high velocity jet stream through a venturi section. Accelerated abrasive particles by water jet improves cutting process. Benjamin Tilghman was awarded a patent in 1870 for cutting stone using abrasive addited water. Today more practical and commercial AWJ cutters are available up to 900 MPa and 1000 m/s (Miller, 2018).

1.1.1.2 Abrasive Slurry Jet

Unlike abrasive feed through a venturi in AWJs, water and abrasive slurry is mixed and then pressurised together through the nozzle. Slurry jets are potentially more efficient than AWJ at the same pressure but current production equipment capacity levels are not much as AWJs (Wilkinson, and Watt, 2006).

1.1.1.3 Cavitating Fluid Jet

A type of special nozzle is used to generate natural cavitation causing bubble formation in fluid flow at relatively low pressures like 70 MPa. Target material is bombarded under these vapour bubbles. Erosion takes place where bubbles collapse and give intense damage to material at impact point (Wilkinson, and Watt, 2006).

1.1.2 Types of Non-Commercial Water Jets

Non commercial water jets are special tools designed for use in experimental setup.

1.1.2.1 Single Impact Jet Appratus (SIJA)

A lead projectile is fired using an air gun to a neoprene diaphragm covering a nozzle which is filled with water. This extrudes a jet of water through the nozzle at velocities up to 1000 m/s (Lopatnikov et al., 2012). In Figure 1.6 diagram of a SIJA is given.

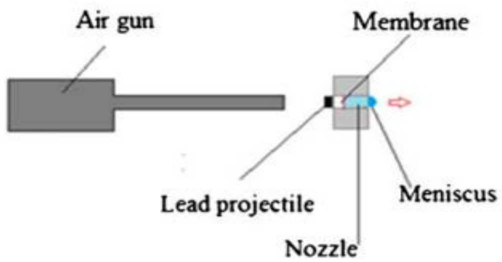

Figure 1.6. Single impact jet apparatus scheme

1.1.2.2 Multi Impact Jet Apparatus (MIJA)

The basic difference from SIJA is the design of the equipment which is not limited with producing a single jet. To provide this, deformable parts of SIJA like membrane is exchanged with a nylon piston and a titanium shaft (Johnson, 2007).

1.1.2.3 Split Bar Water Generator (SBWJG)

SBWJG accelerates water up to 2000 – 3500 m/s velocities by using different acoustic impedance metals. Idea is based on compressing a thin layer of water with two metal bars. In Figure 1.7. structure of a SBWJG is defined. Incident bar is hit by striker bar creating a shock wave in transmitter bar and reflected wave compress water through a nozzle (Lopatnikov et al., 2012).

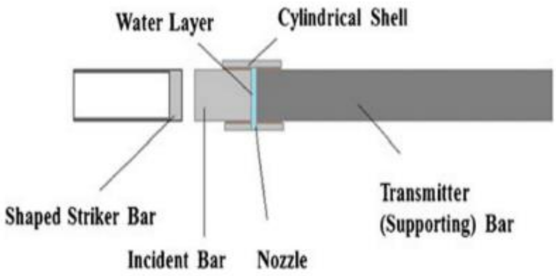

Figure 1.7. Split bar water jet generator scheme

1.2. Pump Types for Pressure Generation

Commercial water jets generally use plunger pumps, intensifier pumps or both, in the name of multistage pumps to pressurize water (Mohamed, 2004).

1.2.1 Plunger Pumps

Plunger pump is a positive displacement reciprocating pump using a stationary seal and cylindrical plunger. Design of the machine allows it to be used at very high pressures such as 200 MPa (“Plunger pump,” 2020).

1.2.2 Intensifier Pumps

Oil and water side piston area ratio is defined as intensification ratio. This ratio determines the capacity of the pump and the value which water will be pressurized is ratio times hydraulic oil pressure. Two-way piston and a directional control valve ensures the continuity of water flow by changing direction and duties. Developing technology enabled pumps having 1:50 amplification ratios creating 1000 MPa (WARDjet, n.d.).

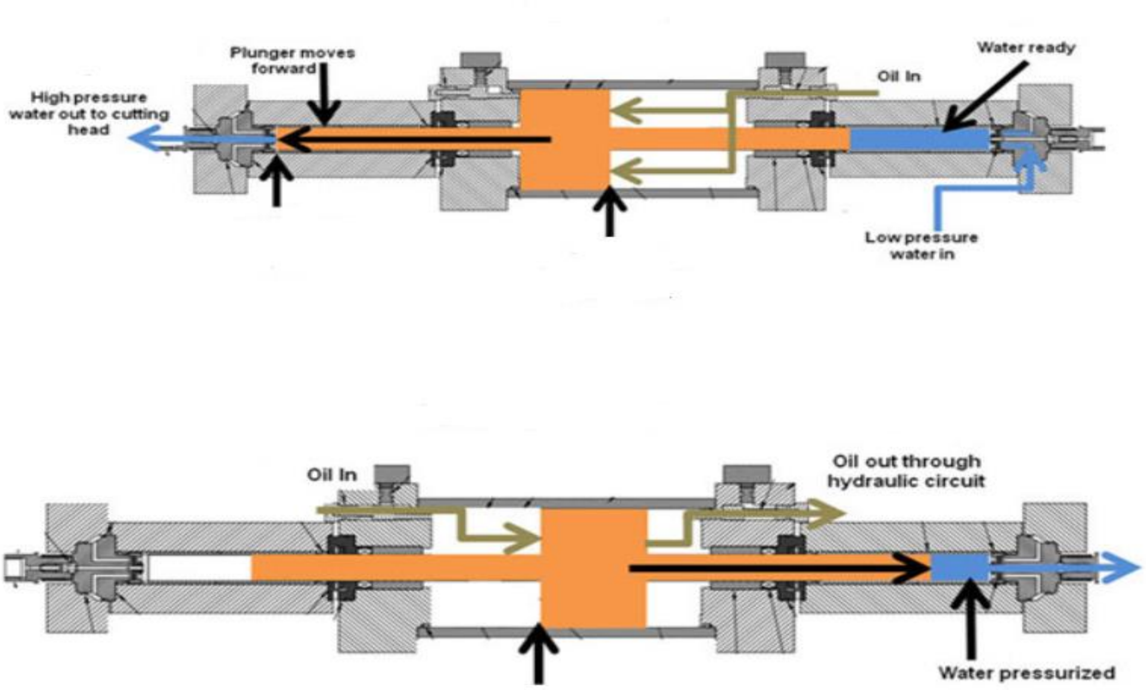

Figure 1.8. Intensifier Pump (Mohamed, 2004)

Figure 1.8. simply describes working principle of an intensifier pump. In this study, intensifier pumps are chosen because it provides and ensures continuous water flow at 150 MPa compared to plunger pumps.

1.3. Behaviour of Water Under High Pressure

Water jet behaviour is investigated to find out flow type and break up mechanisms under high pressure flow.

1.3.1 Flow Type of Water

Fluids are normally considered to be incompressible but high-pressure applications which are bigger than 100 MPa like water jets, this approach will not work. The density of water increases with increasing pressure due to compression (Vasilis, and Solomos, 2013). Density of water due to pressure is given in Figure 1.9.

$$\frac{dp}{E} = \frac{d\rho}{\rho} \quad (1)$$

$$\rho = \rho_0 e^{p/E} \quad (2)$$

E: Modulus of compressibility E=4.07x10E9 N/m^2

ρ_0=1.02103 kg/m^3 (3)

Second formula where; E=3.047x10E8 N/m^2 n=7.15 (Mohamed,2004).

$$\rho=\rho_0\left(\frac{P+E}{P_0+E}\right)^{1/n} \quad (4)$$

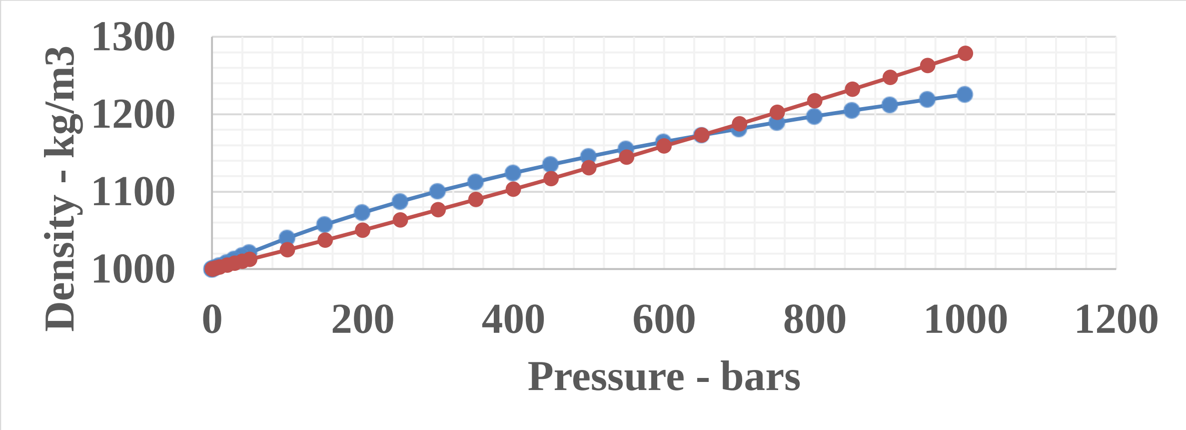

Figure 1.9. Change of Density Due to Increasing Pressure

Compressing water under high pressure requires a lot of hydraulic energy. During jet flow this hydraulic energy is transformed into kinetic energy. Sudden interaction of air and compressed water, which is expanding due to pressure relief, forms a chaotic change in flow structure caused by the change in inertial and viscous forces. In Figure 1.10. flow structure of high speed water is given. Reynolds number is calculated to foresee the behavior of flow and results are shown in Table 1.1. To keep R_e small density, increase due to pressure is neglected. All calculations are based on a 2 mm nozzle.

$$R_e = \frac{\rho v_L}{u} \quad (5)$$

Table 1.1. Re Values of Water Flow Between 0.1-1000 MPa

Pressure - Mpa	Density - kg/m3	Velocity - m/s	Dynamic Viscosity N.s/m2	Section- m	Re
1000.00	1000.00	1414.21	0.001	0.002	2828427.12
950.00	1000.00	1378.40	0.001	0.002	2756809.75
900.00	1000.00	1341.64	0.001	0.002	2683281.57
850.00	1000.00	1303.84	0.001	0.002	2607680.96
800.00	1000.00	1264.91	0.001	0.002	2529822.13
750.00	1000.00	1224.74	0.001	0.002	2449489.74
700.00	1000.00	1183.22	0.001	0.002	2366431.91
650.00	1000.00	1140.18	0.001	0.002	2280350.85
600.00	1000.00	1095.45	0.001	0.002	2190890.23
550.00	1000.00	1048.81	0.001	0.002	2097617.70
500.00	1000.00	1000.00	0.001	0.002	2000000.00
450.00	1000.00	948.68	0.001	0.002	1897366.60
400.00	1000.00	894.43	0.001	0.002	1788854.38
350.00	1000.00	836.66	0.001	0.002	1673320.05
300.00	1000.00	774.60	0.001	0.002	1549193.34
250.00	1000.00	707.11	0.001	0.002	1414213.56
200.00	1000.00	632.46	0.001	0.002	1264911.06
150.00	1000.00	547.72	0.001	0.002	1095445.12
100.00	1000.00	447.21	0.001	0.002	894427.19
50.00	1000.00	316.23	0.001	0.002	632455.53
40.00	1000.00	282.84	0.001	0.002	565685.42
30.00	1000.00	244.95	0.001	0.002	489897.95
20.00	1000.00	200.00	0.001	0.002	400000.00
10.00	1000.00	141.42	0.001	0.002	282842.71
5.00	1000.00	100.00	0.001	0.002	200000.00
1.00	1000.00	44.72	0.001	0.002	89442.72
0.50	1000.00	31.62	0.001	0.002	63245.55
0.10	1000.00	14.14	0.001	0.002	28284.27

It was seen that Re>>2300 for all flow cases through nozzle so flow is fully turbulent

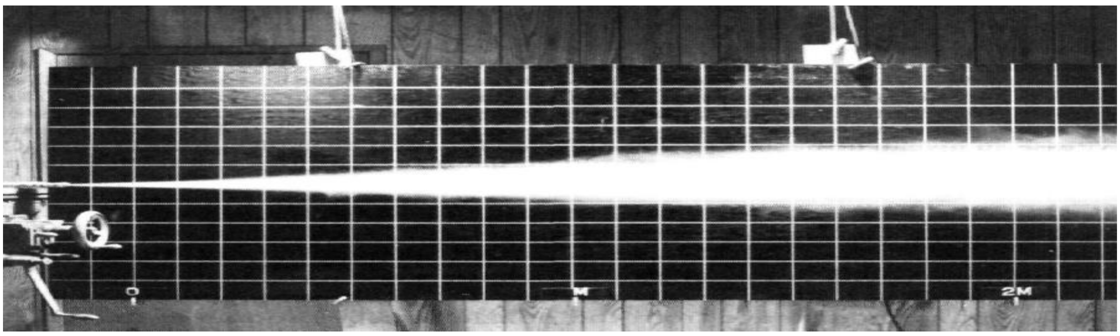

Figure 1.10. Very high velocity water jet movement in air (Rajaratnam et al.,1994).

1.3.2 Break Up Mode of Water

The other dimensionless parameter affecting water flow is the Weber number. We defines different fluids interaciton such as water and air related with velocity and surface tension. In Figure 1.11. break up modes of water is given related with We number.

$$W_e = \frac{\rho v^2 L}{\sigma} \quad (1)$$

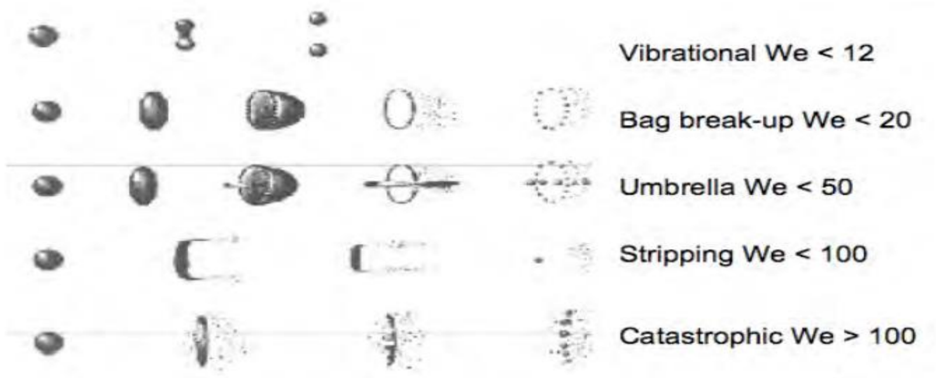

Figure 1.11. Pump Break up modes of a falling water drop (Johnson, 2007).

In order to have a small Weber number, coherent length and jet velocity is taken minimum 0.5 m and 50 m/s respectively. In the best case We>>100 so water breaks up into droplets in a catastrophic manner in the most optimistic case. $\sigma = 0.0727\ N/m$ (surface tension of water) Even if value of L is taken as “1” We number will not be under 100 so the flow characteristic is always catastrophic in this study. In Figure 1.12. distortion process photograps are shown.

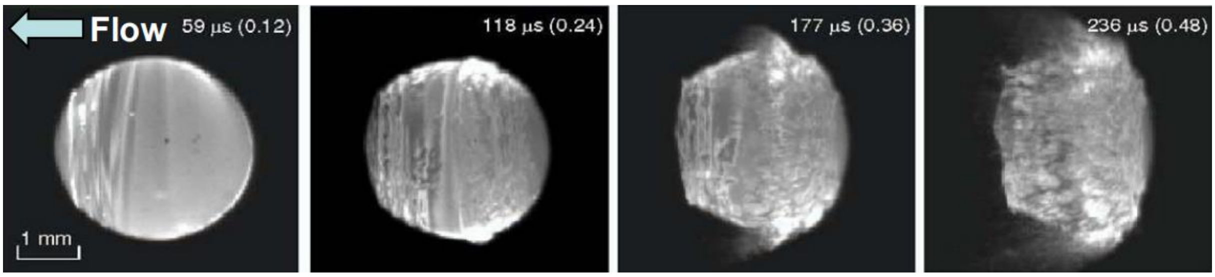

Figure 1.12. Pump Demise photographs the droplet distortion process in a Weber = 5400 flow (Moylan, Landrum, & Russell, 2013).

1.4. Physical Limitations of Water Jets

In order to define simulation parameters, physical limits of water jets are studied and summarized.

1.4.1 Pressure and Velocity Limits

Water freezes at 25 ^{0}C at 1 GPa so for a commercial water jet, 1000 MPa is the upper pressure limit deriving a maximum velocity of 1496 m/s (Miller, 2018).

On the other hand when ice formation under high pressure vs adiabatic heating of water during compression is investigated it was seen that heat produced during flow caused by friction forces prevent ice formation. Taking maximum speed of 1400 m/s would be considered a common sense approach (Mohamed, 2004).

1.4.2 Useful Effective Zone of a High Pressure Water Jet

Process of air entrainment into compressed water jet results in breakdown of water into droplets (Guha et al., 2011). Three main region occurs during this flow. These regions are shown in Figure 1.13. Solid jet after leaving the nozzle disintegrates into droplets and these two is covered with a spray zone which does not have force enough erode the target material (Mohamed, 2004).

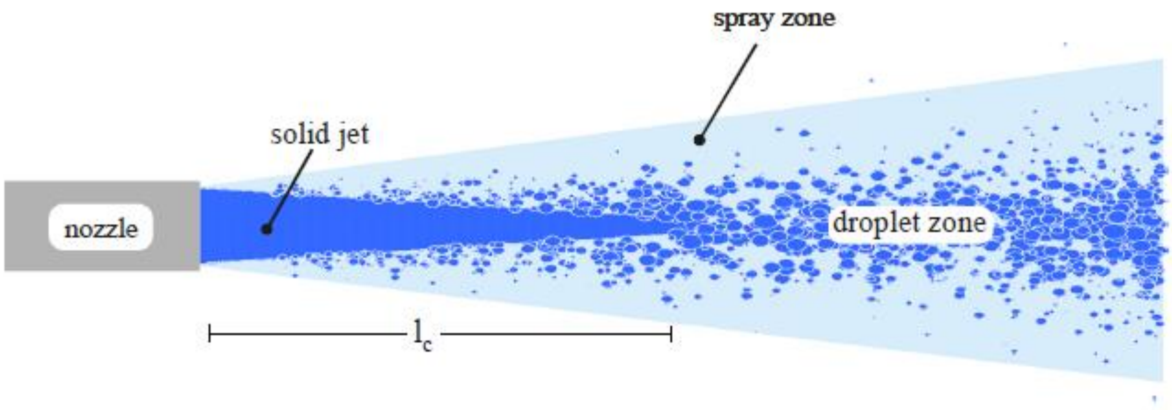

Figure 1.13. High Pressure Water Distribution in Air (Kamel, 2004)

Solid jet length where velocity remain constant is defined as 100D by Rajaratnam (Rajaratnam et al., 1994) where D is nozzle diameter. According to Guha (Guha et al.,2011) radially the jet loses its effectiveness at 1.68D. In the calculations and simulations made in this thesis, the study was carried out by considering the coherent zone / solid jet dimensions.

1.4.3 Power consumption of water jets

Water is assumed to behave like a solid and flow rate, volume and water mass is calculated. Time between collision and water spray is used to determine the average power need. The hydraulic power requirement is calculated and tabulated according to kinetic energy equations and friction loses are neglected to minimize the necessity. Results are given in Table 1.2.

$KE = 0.5.m.v^2$ (1)

$P = E/\Delta t$ (2)

Table 1.2. Power Need of WJ

No	Nozzle Diameter - mm	WJ Velocity - m/s	Collision Point - m	Volume - m^3	Flow Mass - kg	Energy - joule	t - s	p - kW
1	2	150	0.2	6.28E-07	6.28E-04	7.07	1.33E-03	5.30
2	2	150	0.3	9.42E-07	9.42E-04	10.60	2.00E-03	5.30
3	2	500	0.3	9.42E-07	9.42E-04	117.75	6.00E-04	196.25
4	4	150	0.3	3.77E-06	3.77E-03	42.39	2.00E-03	21.20
5	4	500	0.3	3.77E-06	3.77E-03	471.00	6.00E-04	785.00
6	4	500	0.6	7.54E-06	7.54E-03	942.0	1.20E-03	785.00
7	4	500	0.4	5.02E-06	5.02E-03	628.00	8.00E-04	785.00
8	6	150	0.3	8.48E-06	8.48E-03	95.38	2.00E-03	47.69
9	6	500	0.3	8.48E-06	8.48E-03	1059.75	6.00E-04	1766.25
10	6	500	0.6	1.70E-05	1.70E-02	2119.50	1.20E-03	1766.25
11	10	500	1	7.85E-05	7.85E-02	9812.50	2.00E-03	4906.25
12	10	500	0.6	4.71E-05	4.71E-02	5887.50	1.20E-03	4906.25
13	10	150	0.6	4.71E-05	4.71E-02	529.88	4.00E-03	132.47

Results shown in the table leads to slower velocity and higher-pressure values.

1.5. Water Jet and Explosive Interaction

According to Miller's study (Miller, 2018) hundreds of thousands of munitions are discarded using water jets at pressures above 380 MPa. Since the ignition energy of the explosive cannot be provided by water, WJ may be the safest method of discarding energetic material. Initiation energy of PBX9404 explosive and water jet ignition energy is given in Figure 1.14.

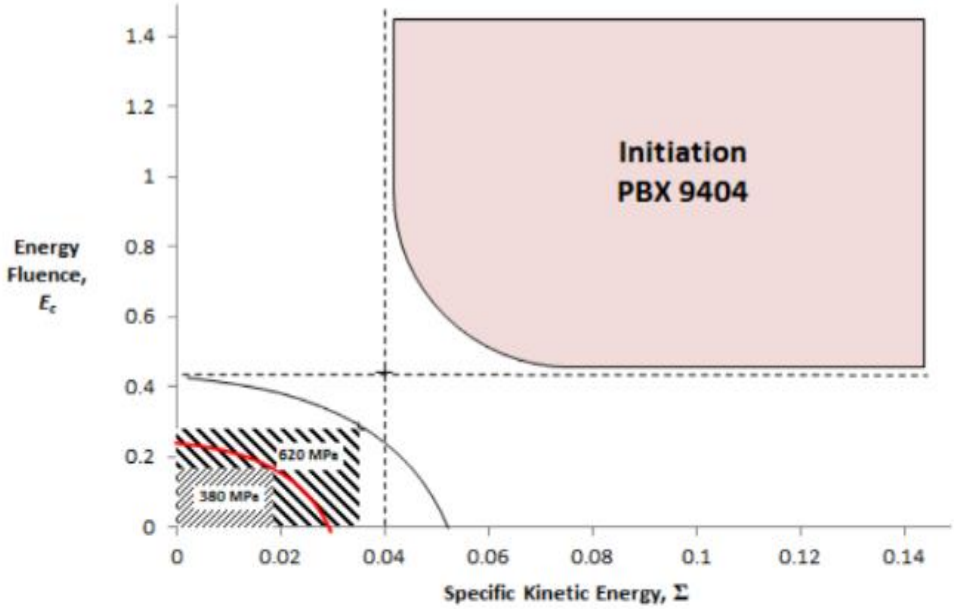

Figure 1.14. WJ Physical Ignition Limits James Criterion vs. WJ Envelope at 380 MPa and 620 MPa (Miller, 2018)

The graph shows that even the highest water jet pressure in the range used in this study has no effect when applied directly to the explosive itself. Therefore, the water jet, which is used as an active protection system, must either activate the fuse directly and detonate the ammunition or divert the ammunition and change the angle of impact.

1.6. Impact Mechanism and Impact Forces of Water Drops

According to Bowden and Brunton's study impact velocities below 500 m/s surface deformation of mild steel become an annular depression zone instead of a fracture. 1.3 mm diameter water jet hitting pressure gauge at 720 m/s caused 630 kg load on the specimen. The distribution pattern is not uniform however average pressure on the impact zone is 930 MPa. Peak value is reached in 1 µs and rapidly deceased in 2 or 3 µs. Steady state Bernoulli pressure and water hammer pressures are compared also. It was seen that Bernoulli pressure of 137 MPa cannot deform mild steel which has a compressive yield strength of 245 MPa. On the other hand calculated water pressure of 1070 MPa is a little higher than the values obtained by the experiments -930 MPa- which are suggested to be caused from surface irregularities (Bowden, and Brunton, 1958). In Figure 1.15. high speed liquid and solid interaction and in Figure 1.16 crack initiation and surface irregularity is visualized. In Figure 1.17 crack deformation of ductile aluminium and brittle zinc is given. In Table 1.3. relevant studies and assumptions made on crack liquid solid interaciton calculations are summarized.

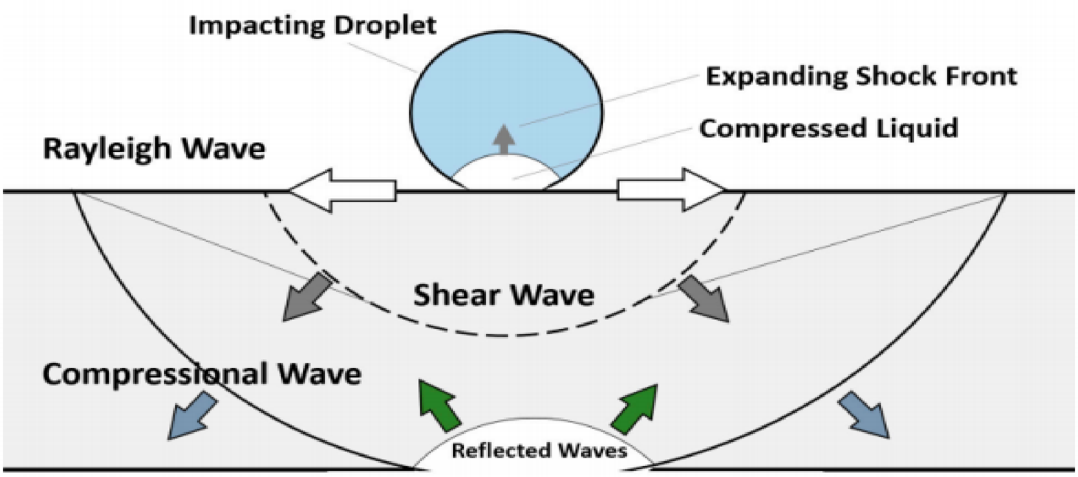

Figure 1.15. Liquid solid interaction (Sibille, and Tasset, 2020)

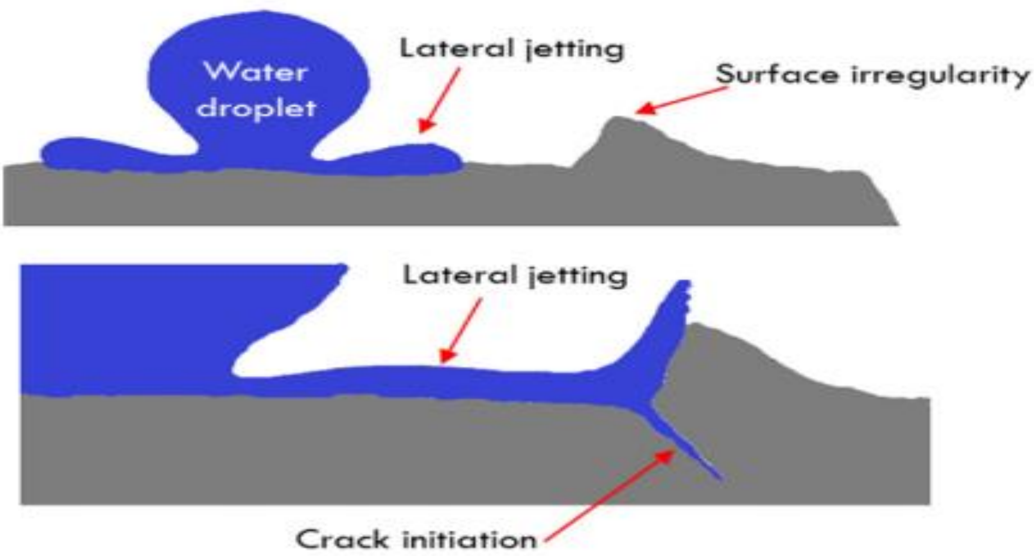

Figure 1.16. Crack Initiation Mechanism of Liquid Solid Interaction due to surface irregularities (Sibille, and Tasset, 2020)

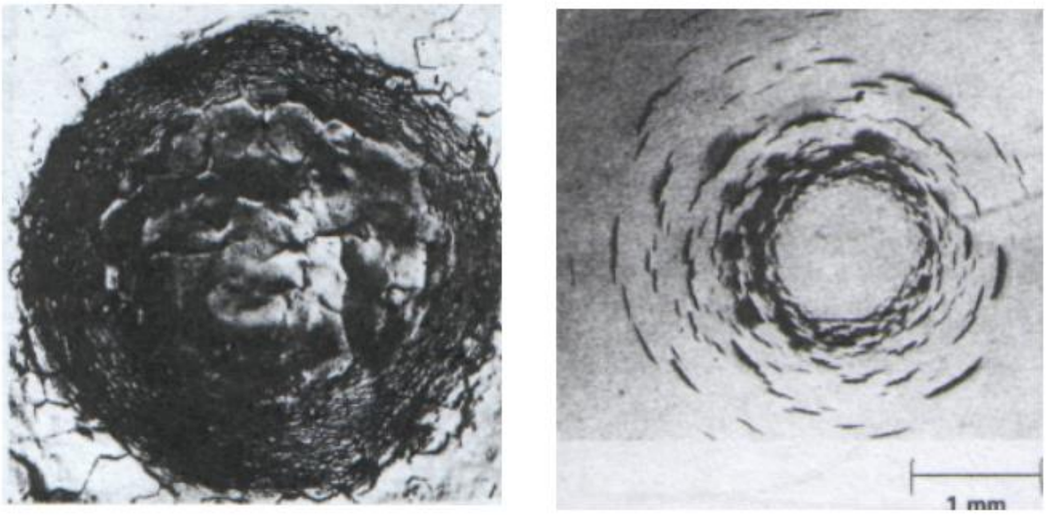

Figure 1.17. Crack Deformation of ductile aluminium left / and brittle material zinc right (Mohamed, 2004)

Table 1.3. Relevant Studies Made on Pressure and Deformation Mechnism (Rochester, 1978)

Impact Pressure Distribution at the Liquid/Surface Interface when a Liquid Drop Strikes a Plane Rigid Solid			
Approach	Drop Shape	Pressure	Pressure Distribution
Theory and experiment - Engel (1955)	Spherical drop	Mean pressure $0.5\rho_0 c_0 v$	Non uniform. Maximum pressure not given but assumed to be in ring around centre of impact.
Theory - Bowden and Field (1964)	Spherical drop	$\rho_0 c_0 v$	Uniform.
Theory, wedge analogy - Heymann (1969)	Cylindrical drop	Max. pressure $3\rho_0 c_0 v$	Non uniform. Maximum pressure about at edge of contact region just before flow occurs.
Theory, wedge analogy - Camus (1971)	Cylindrical drop	Factors of $\rho_0 c_0 v$	Non uniform. Maximum pressure at edge of contact region just after flow starts.
Theory - Huang et al. (1971)	Pin-cushion drop	Max. pressure $0.8\rho_0 c_0 v$	Non uniform. Maximum pressure occurs at centre of impact
Theory - Lesser (1973)	Rectangular slug	Max. pressure $\rho_0 c_0 v$	Non uniform. Maximum pressure occurs at centre of impact
Experiment - Johnson and Vickers (1973)	Cylindrical jet	Max. Pressure $1.5\rho_0 c_0 v$	Non uniform. Maximum pressure occurs at edge of jet.
Experiment - Rochester and Brunton (1974)	Cylindrical drop	Max. pressure $0.7\rho_0 c_0 v$	Non uniform. Maximum pressure occurs at centre of impact.

Recent studies also showed both analytically and numerically that impact pressure occurring at the contact point of solid and liquid can be predicted by $\rho_0 c_0 v$. (Tatekura et al., 2018)

1.7. Forces Acting on a Missile

Li and Hong investigated drag and lift forces on an anti tank missile by changing horizontal and vertical tail fins' angles. In Figure 1.18. pressure distribution is shown. Force value of nearly 230 N is applied to missile during flight. Values are given in Table 1.4. This value is used in estimations made to foresee momentum direction and flight path change.

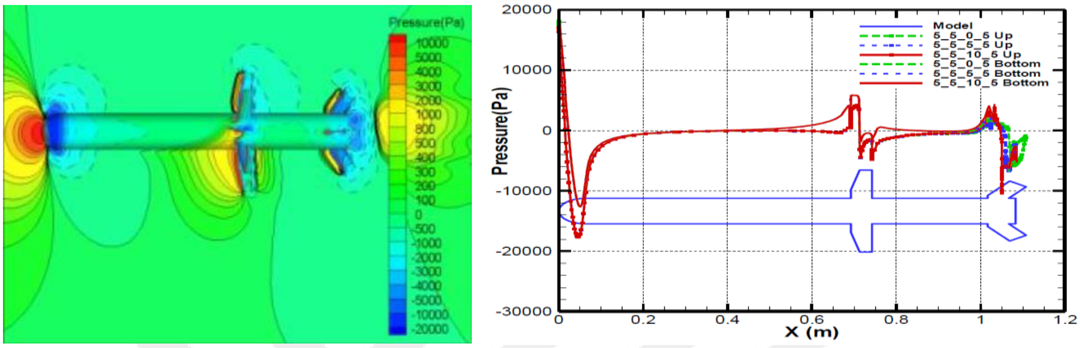

Figure 1.18. Pressure Distribution on a Missile During Flight (Li, and Hong, 2017)

Table 1.4. Forces Acting on Body Elements of Missile (Li, and Hong, 2017)

Term	5_5_0_5	5_5_5_5	5_5_10_5
Head	29.2	29.2	29.19
Cylinder	71.07	70.88	70.56
Back	-4.03	-4.16	-4.45
Win-1	-0.39	-0.39	-0.4
Win-2	17.57	17.65	17.72
Win-3	35.87	35.82	35.76
Win-4	19.76	19.66	19.57
Win-5	-0.02	-0.02	-0.02
Win-6	18.66	18.77	18.89
Win-7	36.03	36.06	36.07
Win-8	19.95	19.86	19.76
Fin-1	-0.65	-0.95	-1.34
Fin-2	-7.04	-7.06	-7.08
Fin-3	0.42	0.39	-0.004
Fin-4	-7.12	-7.18	-7.30
Net	229.28	228.53	226.92

1.8. Force Applied by High Pressure Water

Applied force by high pressure water is researched to understand the effects on missile material.

1.8.1 Force Measurement of Water Cannons

DSTL, examined medical implications of water cannon on human body. Water cannons are used to suppress civil riots by governments in many countries. During actions it has been observed that people were seriously injured because of knock down and debris hitting sensitive organs like eyes. Different spray modes of water cannons is given in Figure 1.19. To analyze the effect, test setup consisting of plates having diameters of 25 to 400 mm is built and struck by pressurized water. Pressure and distance is changed during tests. At 20 meter stand off distance with 15 bar up to 1200 N force is measured. Test setup appratus are shown in Figure 1.20. Average impuls of 125 kg.m/s is also recorded which is enough to knock down a 100 kg man at 7 bar with a 25.4 mm nozzle (The medical implications of vehicle-mounted water cannon with special reference to the Ziegler Wasserwerfer 9000 (WaWe 9) system, 2013).

Figure 1.19. Water Cannons Different Spray Modes.

Figure 1.20. Force Plate Rigs with Pressure Sensors

In theory, without friction loses and maximum efficiency, water jet sprayed through a nozzle with 3 MPa (30 bar) hitting 25 mm and 150 mm diameter plates can exert maximum forces of 1471 N and 52987 N respectively without standoff distance. Here 25 and 150 mm denotes missile radome and body without any aerodynamic design assuming flat and facing pressureised water directly. On the other hand, measuring these forces is impossible due to shock waves occurring on high-speed flights which will obstruct homogeneous pressure and force distribution. This phenomenon is given in Figure 1.21. In this study water cannons will be evaluated together with the nozzle that creates the equivalent force.

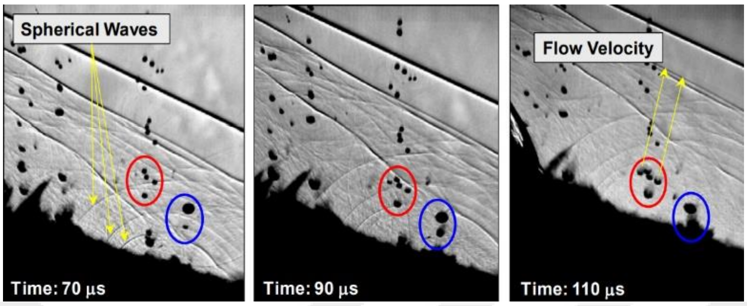

Figure 1.21. Shock Wave and Water Droplet Interaction on High Speed Spherical cone projectile 990 m/s impact (Moylan, Landrum, and Russell, 2013).

1.8.2 Force Measurement of a Commercial Water Jet

Forces exerted on a workpiece by 358.5 MPa abrasive water jet at a flow rate of 8.3 g/s through a 1.2 mm diameter nozzle was measured on mild steel and aluminium which both have 10 mm thickness. It was seen that regardless of material type force is 40 N in the vertical axis reflecting the stagnation pressure of the incident jet. On the other hand penetration time is directly related to material type which is 6 seconds for Al, and 18 seconds for mild steel (Ohlsson, 1995).

When sidefire nozzles are investigated it is understood that because of sudden change in flow direction, turbulence occurs which ends up with pressure loss, a less aligned flow and less efficient cutting performance. So sidefire nozzles and swirling jets are not considered in this study (Hashish, 2009).

1.9. Fuzes

Fuzes are mechanisms used to safe, arm or detonate military munitions. Basic elements of a fuze are responsible for safing and arming, energy storage, event sensing and detonating.

The detonater element triggers the explosive train where a more energetic explosive detonates the end explosive by generating intense pressure waves of 0.724 MPa and more.

1.9.1 Fuze Design Parameters

Cost, size, weight and storage life are some design parameters in fuze manufacturing. Beside these shock and acceleration values are most important because the fuze must not activate during firing when it is subjected to setback forces up to 10^5 g whereas it must activate under the opposite forces occurring at impact.

1.9.2 Types of Fuzes

1.9.2.1 Time Fuze: Activates et the end of a time delay after arming.

1.9.2.2 Impact Fuze: Detonates on impact. It is used on ammunition, bombs and missiles.

1.9.2.3 Delay Fuze: Becomes active after a certain time after impact.

1.9.2.4 Proximity Fuze: Detonates at the closest point of approach to the target (Texas Instruments, 2011, pp.1-8).

1.10. Warheads:

It is the part of the missile, rocket, bomb or torpedo that contains the toxic or explosive substance. Basically, a warhead is comprised of a fuze, an explosive charge and a warhead case. An explosive warhead can cause damage in three ways which are through blast, fragmentation and heat (Wikipedia Contributors, 2019).

1.10.1 Types of warheads

1.10.1.1 High explosive:

It causes damage mostly through blast waves it generate partially fragmentation and lessly thermally. When damage is desired to be fragmentation intended it is designed with a relatively heavy casing.

1.10.1.2 High-explosive fragmentation:

It primarily causes damage by generating high speed fragments. It is employed against personnel and unarmoured vehicles.

1.10.1.3 High-explosive anti tank: (HEAT)

When the explosion occurs, the shock wave causes a very high pressure on the outside of the conical lining. HEAT type warhead components are shown in Figure 1.22. This pressure allows the cone to be extruded and accelerated. During the process, very different velocity profiles are observed such that the tip of the cone moves at 10000 m/s while the rear part moves at 1000 m/s. Due to this difference, the cone moves like a molten metal spear at pressure values up to 40000 MPa. Working principle of a HEAT warhead is given in Figure 1.23. The strike of this spear to vehicle armour results in very high temperatures resulting in melting the armour of vehicle and fusing the hole at the point of contact. The impression is created that the armour is not pierced but is burned through therefore the first hollow charge projectiles were named armour burning missiles (Yevdokimov,1967).

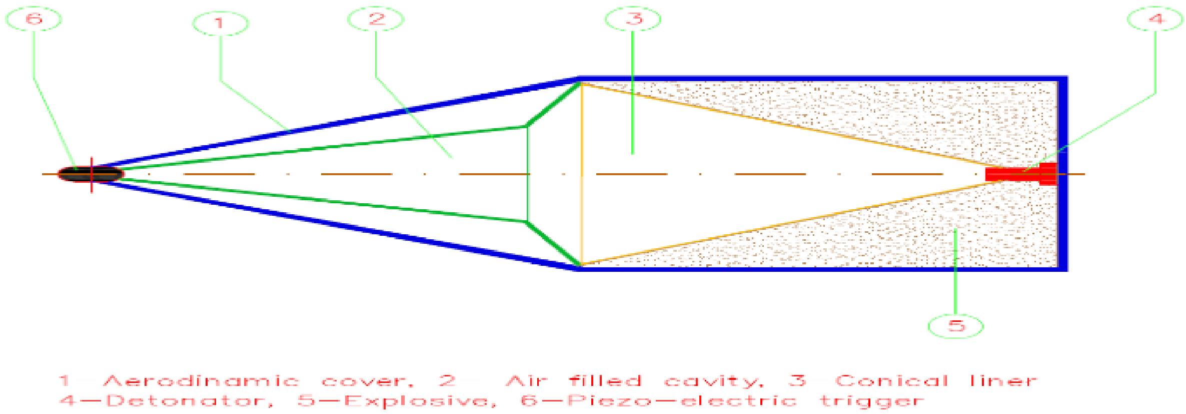

Figure 1.22. HEAT Type Warhead

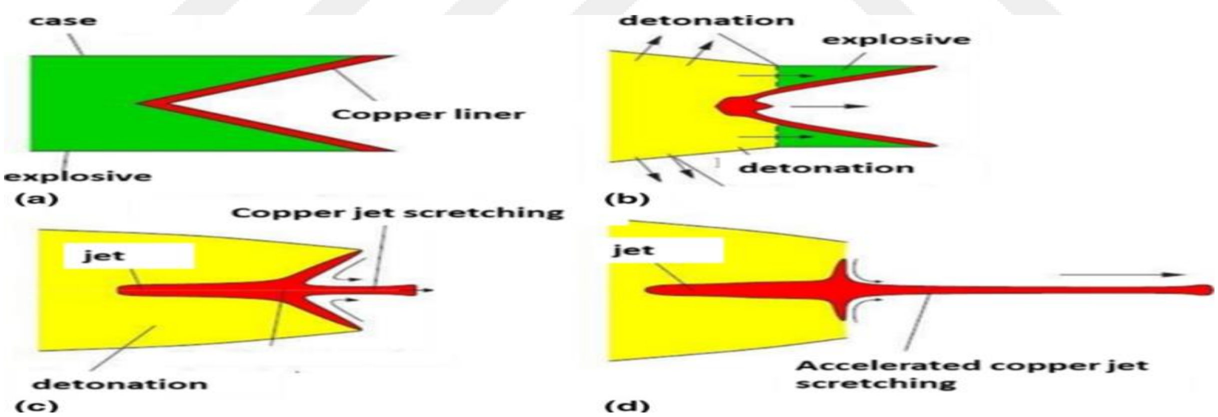

Figure 1.23. HEAT Warhead Working Principle (Baykara, Günay, and Demirural, 2021)

1.10.1.4 High explosive dual purpose:

It is designed to give damage to both personnel and armoured vehicles. This is achived by a pairing HEAT warhead with a fragmentation casing.

1.10.1.5 Thermobaric:

It is manufactured with a certain amount and type of explosive which exploits oxygen in air to strengthen blast wave effects. Duration of shock waves increase from milliseconds to tens of milliseconds. Designed to be used in enclosed spaces like buildings, caves and tunnels. (Jenzen-Jones et al., 2018)

1.11. Power and Effects of an Explosive Charge

Calculation of Blast Loads for Application to Structural Components manual is used for calculating blast pressure and blast impuls. Calculations are made for both 1 kg and 2 kg of charge of TNT with a minimum distance of 0.5 m. Maximum distance is 3 meters. Explosion is assumed to take place in free air and contact angle is assumed to be 60°. Mass of explosive and explosion distance is determined from Figure 1.28. Pressure, time, impuls and velocity values are read from the tables and summarized in Table 1.5.

Two of the charts used, from the related source are given below as Figure 1.24 and Figure 1.25.

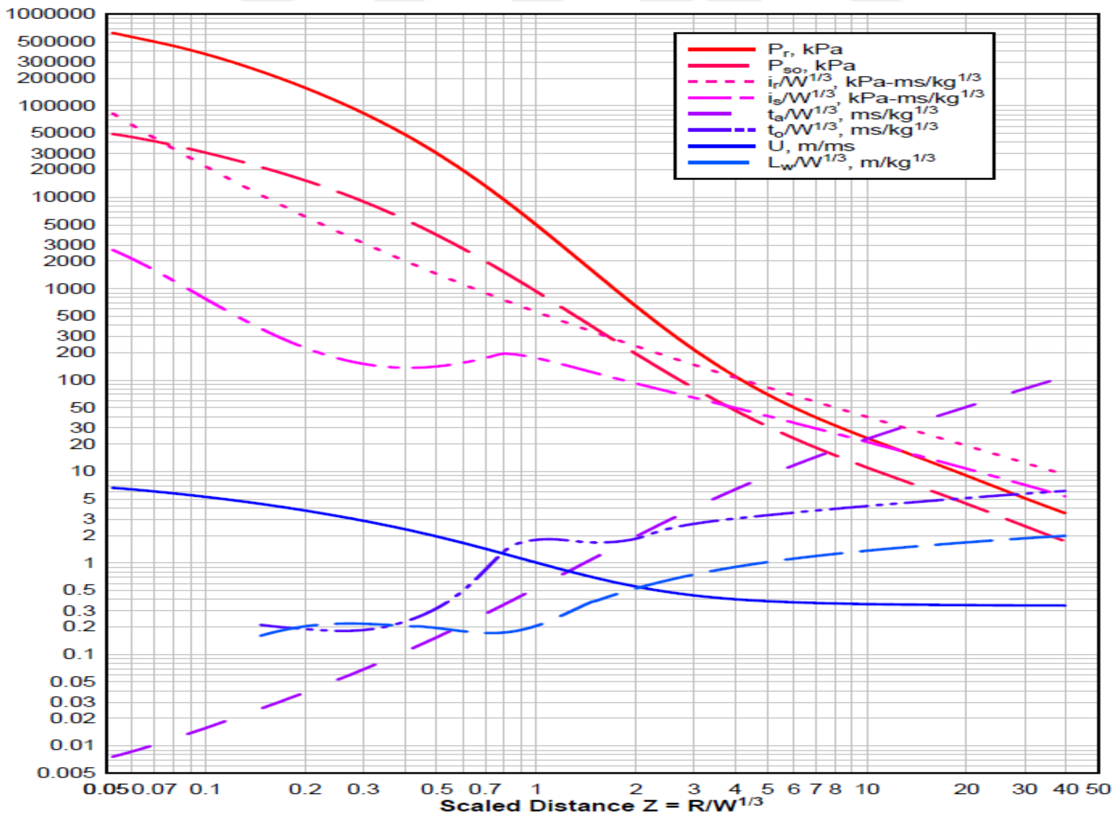

Figure 1.24. Pressure, impuls, time velocity chart due to scaled distance (Vasilis, and Solomos, 2013).

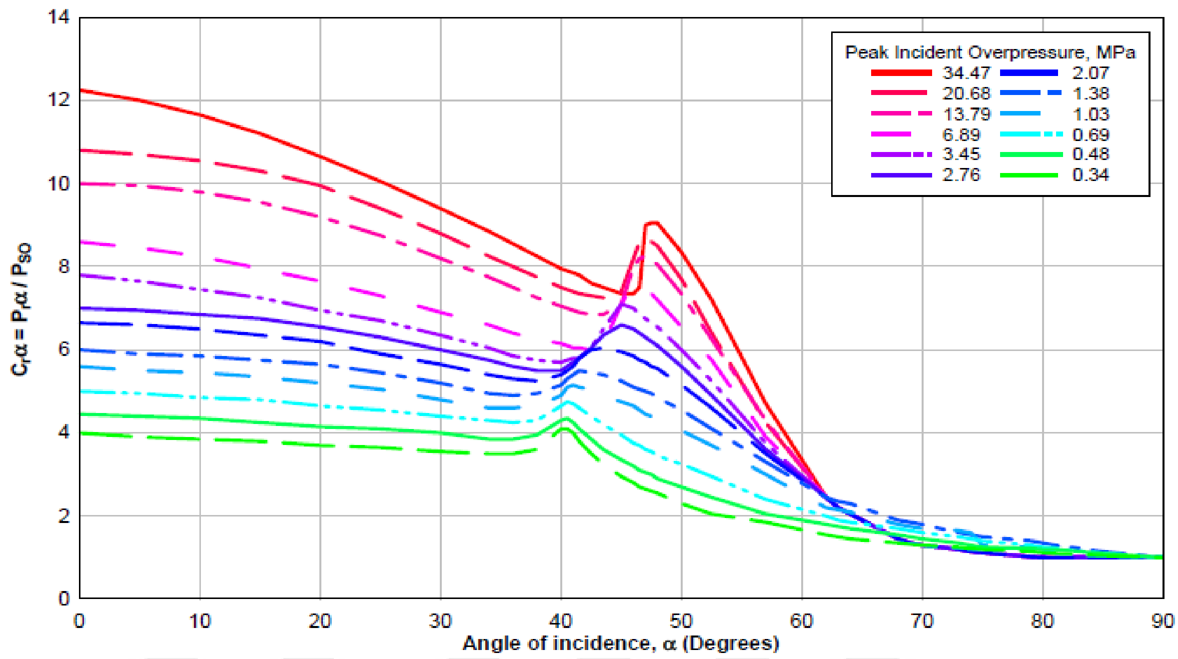

Figure 1.25. Angle of incidence and overpressure chart (Vasilis, and Solomos, 2013).

Table 1.5. Summary of Blast Calculation Results

Explosive Weight - W - kg	Distance - m	Explosive and missile interaction distance - r - m	Scaled distance - Z	Pso - MPa	Crα	PsoM - Mpa	Reflected Impuls - MPa.ms
1	0.5	0.58	0.58	2.70	3.00	8.10	0.24
1	1	1.16	1.16	0.83	2.20	1.83	0.36
1	2	2.33	2.33	0.17	1.65	0.28	0.35
1	3	3.49	3.49	0.06	2.00	0.12	0.33
2	0.5	0.58	0.46	4.30	3.20	13.76	0.27
2	1	1.16	0.92	1.30	1.40	1.82	0.34
2	2	2.33	1.85	0.29	1.60	0.46	0.30
2	3	3.49	2.77	0.08	1.90	0.15	0.25

In Figure 1.26. blast pressure and in Figure 1.27 blast impuls values' graphics are given due to distance.

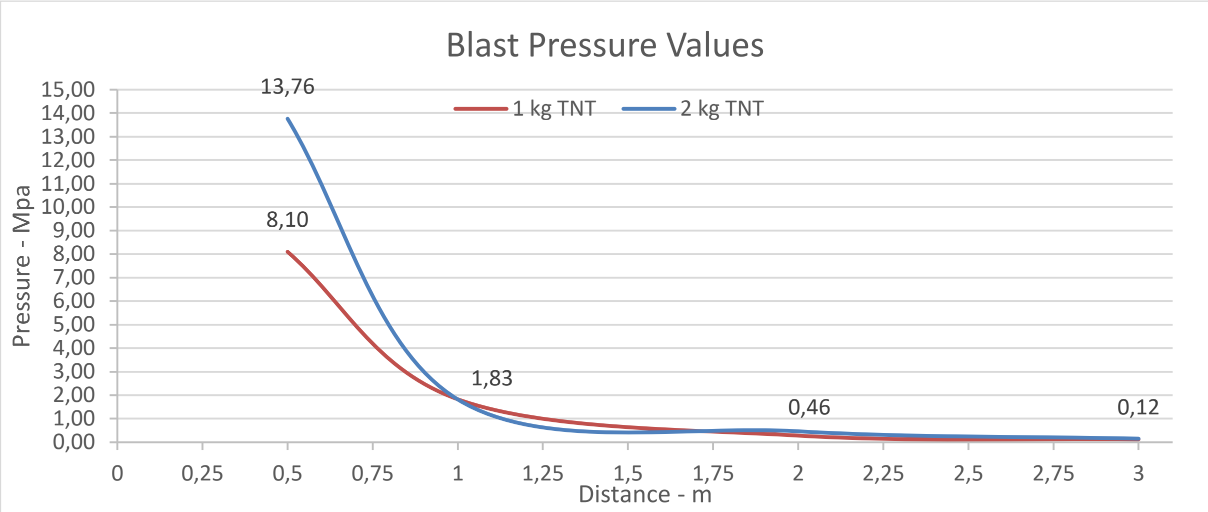

Figure 1.26. Blast Pressure Values Due to Distance

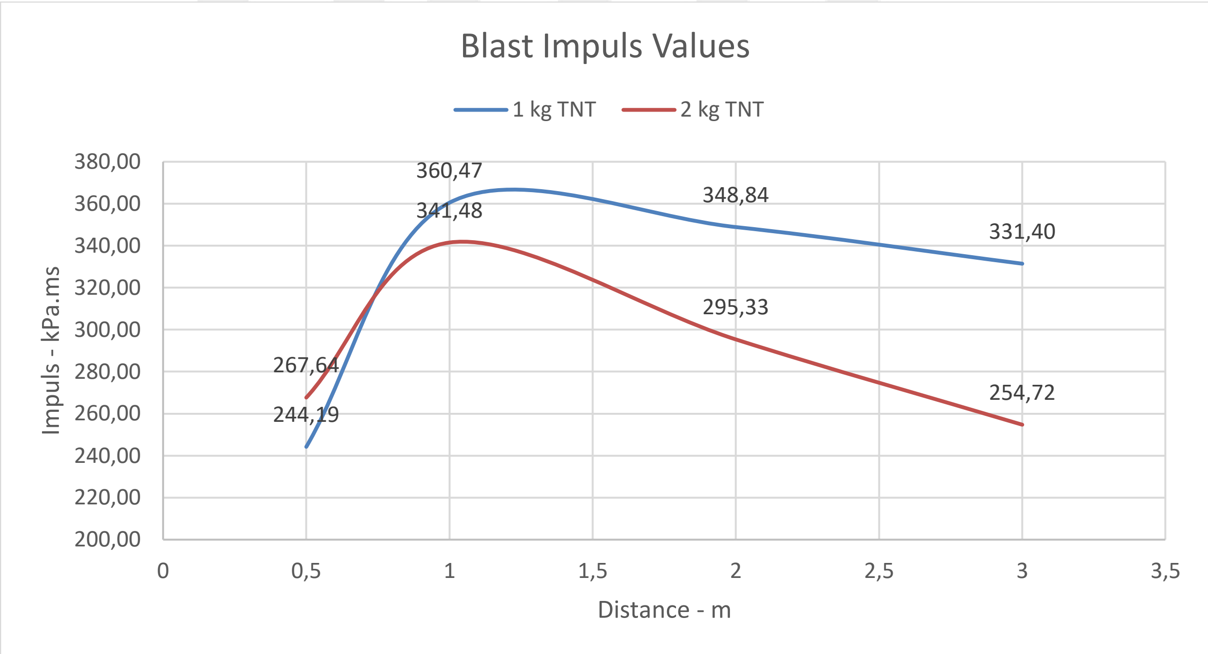

Figure 1.27. Blast Impuls Values Due to Distance

Minimum pressure with a Mach stem is 0.12 MPa for 1 kg TNT at a distance of 3 m.

Maximum pressure with a Mach stem is 13.76 MPa for 2 kg TNT at a distance of 0.5 m.

Min. Impuls value is 0.24 MPa.ms at 0.5 m for 1 kg TNT.

Max. Impuls values is 0.36 MPa.ms at 1 m for 1 kg TNT.

Second value triggering explosion is the momentum affect of fragments travelling at a speed of 1600 m/s. Fragment mass is 2 g. Fragment moving at 1600 m/s with a mass of 2 g has a momentum of 3.2 kgm/s.

Pressure, impuls and fragmentation momentum values are calculated since there is no source sharing missile explosive design parameters. Related values are compared with the simulation results to figure out water jet effect on missile radome and fuze.

Dome material pyroceam and most of the surface Aluminum 2219-T81 (Fleeman, 2001)

Aluminum tensile strength 352 MPa

Shear strength 285 MPa (“ASM Material Data Sheet,” n.d.)

Fig.1.28 Counter APS Amno Against an AT-Missile (arronlee33, 2014)

To determine force duration Frost’s studies (Frost et al., 2007) are investigated. In Figure 1.29. high speed photographs of an explosion is given.

Figure 1.29. High speed photographs of the explosive dispersal of 275 μm steel particles from an 11.8 cm diameter charge. Times are 0, 40, 80, 160, 240, 360, 560 and 840 μs respectively (Frost et al., 2007).

Table 1.6. Anti-Tank Missiles

Name		**Citafe Motogo** (Argentina)	**Norinco Red Arrow 8** (China)	**Aerospatiale Eryx** (France)	**Aerospatiale SS.11** (France)	**Euromissile HOT Aerospatiale SS.11** (France/West Germany)	**Euromissile MILAN Aerospatiale SS.11** (France/West Germany)	**MBB Mamba** (West Germany)	**MBB Bö 810 Cobra 2000 Mamba** (West Germany)	**IMI Mapats** (Israel)	**Kawasaki Type 64** (Japan)
Type		Ground-launched short/medium range anti-tank missile	Ground-launched short/medium range anti-tank missile	Man portable short range light anti tank missile	Ground. vehicle or helicopter launched medium range anti tank missile	Ground. vehicle or helicopter launched long range heavy anti tank missile	Man portable ground or vehicle launched short/medium range anti tank missile	Man portable short/medium range anti tank missile	Man portable short/medium range anti tank missile	Ground and vehicle launched long range heavy anti tank missile	Ground. vehicle and helicopter launched short/mediu m range anti tank missile
Dimensions	**Diameter**	0.102 m	0.12 m	0.16 m	0.164 m	0.165 m	0.9 m	0.12 m	0.1 m	0.148 m	0.12 m
	Length	0.998 m	0.875 m	0.905 m	1.2 m	1.25 m	0.769 m	0.955 m	0.95 m	1.450 m	1.00 m
	Span	Not known	0.32 m	Not known	0.5 m	0.312 m	0.265 m	0.4 m	0.48 m	Not known	0.6 m
Weights	**Total Rounds**	11.3 kg	11.2 kg	11 kg	29.9 kg	23.5 kg	6.65 kg	11.2 kg	10.3 kg	18.5 kg	15.7 kg
	Warhead	Not known	Not known	3.6 kg	Not known	6 kg	2.98 kg	2.7 kg	2.7 kg	3.6 kg	Not known
Performance	**Speed**	325 km/h	365 km/h	72 km/h	685 km/h	865 km/h	720 km/h	505 km/h	305 km/h	1135 km/h	305 km/h
	Range	350/2100 m	100/3000 m	---/600 m	500/3000 m	75/4250 m	25/2000 m	300/2000 m	400/2000 m	---/4000 m	350/1800 m
Guidance		Wire command to line of sight	Wire semi-automatic command to line of sight	Wire semi-automatic command to line of sight	Wire command to line of sight	SAT/Eltro wire semi-automatic command to line of sight	SAT/Eltro wire semi-automatic command to line of sight	Wire command to line of sight	Wire command to line of sight	Laser beam-riding	Nihon electric wire command to line of sight

Table 1.7. Anti-Tank Missiles and Warhead Momentum (Chant, 2013)

Name	Citafe Motogo (Argentina)	Norinco Red Arrow 8 (China)	Aerospatiale Eryx (France)	Aerospatiale SS.11 (France)	Euromissile HOT Aerospatiale SS.11 (France/West Germany)	Euromissile MILAN Aerospatiale SS.11 (France/West Germany)	MBB Mamba (West Germany)	MBB Bö 810 Cobra 2000 Mamba (West Germany)	IMI Mapats (Israel)	Kawasaki Type 64 (Japan)
Mass Total - kg	11.3	11.2	11	29.9	23.5	6.65	11.2	10.3	18.5	15.7
Mass Warhead - kg	Not known	Not known	3.6	Not known	6	2.98	2.7	2.7	3.6	Not known
Speed- m/s	90.28	101.39	20.00	190.28	240.28	200.00	140.28	84.72	315.28	84.72
Momentum - kg.m/s	1020.14	1135.56	220.00	5689.31	5646.53	1330.00	1571.11	872.64	5832.64	1330.14
Momentum of warhead - kg.m/s	Not known	Not known	72.00	Not known	1441.67	596.00	378.75	228.75	1135.00	Not known

2. LITERATURE REVIEW

In order to direct the study, research was conducted on both water jets, explosion mechanism and active protection systems. Beside this, literature was reviewed to understand the power of missiles and calculate the force enough to stop, divert or detonate the missile before impact. As the research improves it was seen that exact data was not shared because of national confidelity so physical values are gathered through articles and engineering assumptions are made. The physical strength of water jet was also investigated to compare the data. In the following, relevant studies from the literature can be seen.

2.1. Dynamics of Explosion and Active Protection Systems

Gurney (1943) studied on the effectiveness of a projectile due to initial velocity of a fragment in terms of charge (C) and weight (M) ratio of a projectile. Theory based on the idea that total kinetic energy created by explosion is free of the size of the projectile. For certain domain it was seen that his assumption makes sense. His avant-garde work influenced many other scholars following him made his definitions named as Gurney cylinder and Gurney constant afterwards.

Meyer (1998) wrote an article about active protection systems (APS) and their necessisity. Working principles of the system are given on the reaction time and distance based. Various types of APS's and their capability to engage and stop a missile are given in his work. Also economic parameters and future trends are revised.

Jacinto et al. (2001) investigated plates under blast loads both experimentally and numerically which serves to measure the accuracy of calculation methods. Linear dynamic loads analyses are carried out using ABAQUS. Experiments are made with two plates one is clamped in soil and the other clamped in four edges. The exploasing loads causing pressure waves are recorded and compared with numerical results. Time acceleration and pressure histories are drawn. It was also seen that different vibration modes have crucial affects on pressure distribution which can not be neglected.

Janzon et al. (2007) researched trends in weaponry and warfare, energetic materials and protection. Warheads are analyzed in a detailed way and predicted to be some way multi-purpose in the future. Signs of high-pressure jets through multiple nozzles as a counter measure in close combat as a hard kill system are seen in the study. Also customizable liquid armour is mentioned in the study which's rheological properties can be changed with electrically.

Tai et al. (2007) studied on the effects of blast waves on wheeled armoured vehicles numerically. Flow is assumed to be three dimensional and incompressible. This study is giving certain pressure and time values which are compatible with most of the calculations of aerodynamic characteristics of an anti-tank missile. A maximum of 20 MPa is reached within a 25 ms period.

Chant (2013) gave valuable details about weapons deployed by modern armies like main battle tanks, anti tank missiles, air-crafts and warships in the book "A Compendium of Armamants and Military Hardware".

Karlos and Solomos (2013) worked on the behaviour of structures under sudden pressure and impact changes. Spherical and hemispherical blast effects are inspected according to charge mass of explosive and distance to building. Kinney, Brode, Mils, Newmark and Kingery-Bulmash blast peak pressure approaches are compared. Side on pressure and reflected pressure are counted in.

Luo et al. (2015) analyzed riot bombs fragments injury effects. The quantity and mass distribution and velocity of fragments are evaluated with Gurney equations and compared with the values calculated in PREPOST. It indicates that fragmentation generally give harm below the legs of people. A safe distance is established at the end of the research.

Wey et al. (2016) describes hard kill protection and active protection systems. Their study is about analysing the effectiveness of using an open software "Athena" which was used with Russian defence system Arena. Defined fragment mass is 2 g and velocity is 1800 m/s. The momentum of the fragment is enough to activate the missile. Gave valuable information necessary for design and comparison of water jet capability.

Feickert (2016) who is a specialist in military ground forces defined AP systems briefly. APS must be successful to be fully applied to the armoured combat vehicles in the scope of modernization plans. The need for APS is explained as the threats are becoming inexpensive, easily available and can be used with little training. Continuous development made some of the threats tandem warhead which can easily defeat the reactive armour of MBTs. Defined basic APS considerations, theory and compared products of different nations existing in the same frame. Emphasized importance of a faster system in order to increase number of target variations which could be detected and destroyed. Reaction time is a critical parameter in WJ's contact moment with target defining the distance and trajectory.

Li and Hong (2017) worked on aerodynamic characteristics of an anti-tank missile. According to wind tunnel experiments missiles having eight middle and four tail fins shows superior flight dynamics in the subsonic range. Lift coefficients are examined and static pressure countour of missile surface are calculated. It was seen that with higher lift to drag coefficients missiles are performing more stable flight and much more lethal against armoured vehicles. Maximum pressure of 10000 Pa (0.01 MPa) at missile radome and net lift force of approximately 230 N is calculated. Study is executed using CFD modelling. According to simulations most of the lifting work is done by the middle fins. Define lift/drag ratio for optimum design.

Song et al. (2018) investigated the working sequence of an APS which must be capable of detecting the basic characteristics such as speed and size of the approaching threat. The system must also be able to track the threat and identify the point of impact than send the data obtained to the controller for counter-attack. Disadvantage of the system is milimeter wave radar use which can only respond to typical anti-tank missiles and can not detect high speed kinetic energy missiles. To come over this problem and increase reliability of the detection devices multi-sensor detection and data fusion method is advised which also reduce the false alarm probability.

2.2. Dynamics of High Pressure Water

Engel (1955) worked on water solid impact interaction. Flow of water on solid surface was observed wth the help of acid base reactions. It was seen that collision happens in an oscillatory motion way because of inertia, surface tension or viscosity. Damage pattern on solid is mostly familiar in all kinds os specimen. During experiments cavitation was suspected because change in the direction of water flow ends with a sudden pressure decay in waterdrop centre also. Another reason is shock wave oscillation effect on pressure drop. This is verified with Argon saturated water collision tests and bubbles were observed. Tests are made with different solid surfaces, and it was seen that splash characteristics vary. Pressure and velocity time formulas are evaluated also which makes Olive Engel a prominent and frequently referenced name on this topic.

Bowden et al. (1958) projected a 1 mm diameter and 20 mm long water against a solid surface at a speed of 1067 m/sec. The mass of water is nearly equal to a large raindrop. The break-up of water because of air friction is photographed within periods of 25 μs. Deformation is defined in two stages one is depression zone occurring at the contact point called the central pit and the other an annular region. Because of the direction change in flow, velocities are seen 2-3 times greater than impact velocity. The study concluded that pressure on contact zone is much greater than most materials yield strength raindrops can easily deform materials as hard as tungsten carbide.

Leach et al. (1966) studied on the behaviour of water jet. The aim of their work is decreasing the hazard of spark induced explosion of methane in coal mines. To find out stagnation pressure a transducer adopted to a steel bar with a diameter of 0.3 mm was used. The system was modified from an old lathe so plate distance to jet can be arranged. Jet pressures are measured according to nozzles having different geometry and distance. When the relationship between pressure and distance values is examined, it is seen that the pressure value measured at the sensor at 350D (where D is nozzle diameter) is half the pump pressure. In addition, the pressure value approached to zero at a 2.6 jet radius in the radial direction. This study is important for considering the calculation distances in the simulations carried out.

Heymann (1969) presented a two dimensional model of liquid-solid impact instead of one dimensional mostly used in the relevant literature. Lateral velocities exceeding impact velocity by a factor of 2-5 are observed experimentally. Correlation between critical pressure and instantaneous impact pressure is given and the ratio is nearly 2.8. The range is compatible with experiments done in steam turbine blades erosion. Repeated impact and damage mechanism is mentioned also in this study. Although every impact occurs in a changed surface pressure mechanism is also coherent with the defined range.

Hashish and duPlessis (1978) tried to put forth a theory for penetration of water jets into solid materials. In order to simplify solid-fluid mechanic equations a rheological model for material is chosed which permits appropriate description of a compressive yield strength, damping and hydrodynamic friction coefficient. A formula of cutting is derived at the end of the study.

Brunton and Rochester (1979) investigated erosion mechanism of solid surfaces under liquid drops' impacts. Several parameters such as drop size and shape, solid and liquid materials specifications, impact velocity and angle, surface roughness and coatings' effects are detailly described in their study. Erosion mechanism and weight loss relations are given numerically for different conditions of impact. Precursors' studies about water hammer pressure is also evaluated.

Ohlsson et al. (1994) studied the forces exerted on aluminium and mild steel workpieces. Measured penetration under certain parameters such as standoff distance, nozul diameter, pressure, workpiece thickness and water flow rate. Till penetration force is proportional to stagnation pressure of the incident jet. Numerical data achieved from this study is valuable in comparing computational results with reality.

Rajaratnam et al. (1994) examined behaviour and interaction of high velocity of water jet in air. Evaluated formulas for velocity of water jet related to nozzle diameter and target distance ratio. Velocity profile and decay was obtained in terms of distance and initial velocity at the nozul exit. Effective range of high velocity coherent water jet core is defined. The water velocity is constant up to 100D where D is defined as nozzle diameter. On the other hand at 100D water volume is only %5 of the beginning value.

Adler (1995) modelled the waterdrop impact using three-dimensional finite element method to understand the collision mechanism during contact with a deformable target. Although the pressure and momentum exchange is successfully modelled it was mentioned that there is no such absolute definition about hydrometeor and deformable object interaction.

Wilkinson and Watt (2006) explained methods of disposing energetic material. Under the title of mechanical methods, fluid, abrasive fluid, abrasive slurry, cavitating slurry, water and slurry jets are defined. Parameters affecting jet performance are listed as pressure, nozzle design, abrasive type size and feed rate. It was seen that up to 350 MPa - giving a velocity of 836.6 m/s - water jets are acceptably safe with regard to impact sensitivity and more than one million munitions are discarded by this method without incident.

Lee et al. (1999) investigated TiN coated steam turbin blades water drop impact erosion resistance. A high impedance coating material was chosed to lower the impact stress which has a high density times sound speed value. High impedance decreases the shock wave's destructive depression stress and extend main material life. Relation between impact number of water drops and damage depth is also investigated. They declared as coating thickness increases resistance of material improves and defined a lower limit value for coating thickness.

Bailey et al. (2006) investigated effects of water on blast waves. TNT charges of 0.9, 2.2 and 3.2 kg are exploded with and without water mist usage. Impuls and pressure values are compared and lower values are measured with the hydrated system. It is certain that water mist is suppressing explosive blast waves and its relative damage. This study is important for one other reason because it gives certain values about peak over pressure measured during explosion induced from a known mass of TNT.

Kmec et al. (2010) defined traditional disposal methods of munitions as burying, blowing and burning. Besides introduced hydroabrasive liquid stream cutting as an environmental friendly munition discarding new method which is also safe due to spark prevention during cutting process. Because of its chemical neutraulizing effect ammonia is suggested as an alternative cutting fluid. Safety measures are considered due to spark igniton of abrasives friction with material which could trigger the explosive.

Lopatnikov et al. (2012) looked for an inexpensive rain erosion test method creating milimeter size droplets at high speeds. The most common ways of understanding high speed rain exposure of samples are the sled test and the rotating arm apparatus. Centrifugal affect of the rotating arm moves through artificial rain speeds at 45-290 m/s. Rain affect is developed by using water tank, manifolds and capilleries. In sled test rocket reaches hypersonic speeds such as 1500 m/s passing through a 1800 m rain field. Spray heads create desired droplet distribution. Single Impact Jet Apparatus (SIJA) was used in 1950s to accelerate water to high speeds using external explosion. An air gun fires a lead slug to a sealed nozzle which extrudes water in a jet form having speeds up to 1000 m/s. Split Bar Water Generator (SBWJG) accelerates water up to 2000 – 3500 m/s velocities by using different acoustic impedance metals. Idea is based on compressing a thin layer of water with two metal bars. Incident bar is hit by striker bar creating a shock wave in transmitter bar and reflected wave compress water through a nozzle. This method is superior to sled test because in sled test whole specimen is affected of the rain zone and examinations are vague compared to SBWJG which is giving point analysis. This study also mentions high pressure water interaction with air and shock waves. Highly compressed water explodes to release the elastic energy stored and produces a spray zone turning the jet into a cloud. Realization time is 2 to 5 ms.

DSTL (The medical implications of vehicle-mounted water cannon with special reference to the Ziegler Wasserwerfer 9000 (WaWe 9) system, 2013) investigated the medical implications of water cannon on human body. It was seen that high pressure water can give harm by knocking down the person, debris accelerated by water cannon directed to the ground hitting sensitive organs like eyes and contact of the head with a rigid object like a wall or ground. In order to model the events plates having different diameters are exposed to pressurized water at different distance. Test method seems simple but inspiring for this study. DSTL biomedical sciences researched medical implications of vehicle mounted water cannons affects on riot/people. Using 25-50-100-200 and 400 mm diameter plates at 5-10 or 15 bar force is measured using sensors. At 20 meter stand off distance with 15 bar up to 1200 N force is measured.
Surface tension of water vs eddy currents according to high Reynolds numbers are considered. An average force of 625 N applied for 0.2 s is creating a momentum of 125 kg.m/s which is enough to knock down a 100 kg man at 7 bar with a 25.4 mm nozzle.

Gauert (2013) prepared a report on high pressure waterjet using in underground mining. Under 350 MPa using two different abrasives agents garnet and ferrosilicon with different piercing times cutting depths are measured. Penetration times of waterjet into material is also observed. Cost benefit analysis of waterjet is made and compared with conventional drilling and selective blast mining. It was seen that applying a hybrid model will be the most appropriate way.

Moylan et al. (2013) worked on the fact associated with rain impacts on supersonic and hypersonic vehicles which brought significant design challenge to missile domes and spherical cones. This study highlights that droplet environment of actual flight is a function of vehicle geometry, velocity, shock entry location and duration of interaction. Distortion process of droplets is investigated at We=5400. As a future research it defined impacting droplets disrupting affects on vehicles bow shock which alters aerodynamic boundary region.

Mohamed (2014) in his Ph.D. thesis defined most of the design parameters of high-pressure abrasive water jets. His study also investigates ice formation under high pressure vs adiabatic heating of water during compression which concluded with ignoring the ice formation risk.

Trettel and Ezekoye (2015) worked on the trajectory of a water jet both numerically and experimentally and derived formulas for vertical and horizontal movement of the jet. Break up distance of water due to interaction with air is counted in calculations. Range is increased with decreasing nozzle Froude number, besides under a certain Froude number no break-up is observed where the flow is happening like a dragless particle. The study is important in designing efficient fire protection systems such as hoses and sprinklers.

Medan (2016) searched systems of predicting the efficiency of nozzle. In order to do this the impact force applied on a flat and rigid surface at a certain distance by water jet is measured. After measurement the coherent core of jet velocity is calculated for 1 mm, 1.5 mm and 2 mm nozzle diameters. Using a drain pan flow rate is measured and compared with the theorical results. He defined discharge, speed and contraction coefficints for nozzles and for optimiziation of nozzle efficiency. Measured flow rate is nearly 70 % of the theory which could lead calculating flow rates of water at 1000 bar level. Between working pressure values of 100 to 200 bar, best results are obtained at 180 bar.

Guha et al. (2016) searched axial and radial effective distances of a water jet system used in cleaning to improve in industrial manufacturing processes. Influenced by Rajanatrams's work. When standoff distance is smaller than 5D, where D is nozzle diameter rebounding water is adversely affecting the jet formation and harm the nozzle. At 26D jet loses its cleaning ability and at radial 1.68D debris can not be removed by the jet.

Miller (2018) investigates the safety concerns of discarding munitions using high pressure water jets covering initiation mechanisms trigger such as mechanical, thermal and electrostatic discharge. Patent of abrasive water jets are awarded in 1870. Military combat and tactical applications of water jets are given briefly. First war’s munitions were demilitarized using water jets in 1920s. Safety concerns of using water jets are discussed. In root cause analyses made after accidents that happen, it was seen that WJ is the safest method that can be used in discarding process. Far beyond commercial WJ systems a shaped charged explosive was used to accelerate the water concluding the lowest velocity causing a reaction is 7100 m/s. Energy fluence, initiation energy and spark ignition are considered and WJ impact is unlikely to initiate the explosive.

Literature studies were examined in 2 groups. Active protection systems and explosion dynamics were studied in the 1st group, and water jets in the 2nd group. In this study, unlike the literature, the effect of water jets on ammunition through different parameters (nozzle diameter, fluid velocity, collision distance) when used as an active protection system was examined.

3. MATERIALS AND METHODS

3.1. Understanding Active protection systems

Active protection system neutralizes anti-tank missile in two ways:

1. High velocity fragments hitting the missile
2. Shock wave propogation according to counter-attack, facing the missile

Design parameters and threshold values activating warhead are not shared in literature so basic blast calculations are made to understand how much pressure a counter measure projectile creates and momentum of fragments exploding the missile.

High pressure water jets' impuls and resultant momentum values are simulated and compared with blast calculations. Also water cannons of Somati and Ziegler test results are evaluated.

3.2. ANSYS-LS Dyna Mathematical Model

Model is based on explicit analysis because the investigation is made on high speed, high energy materials on a very short time interval. Missile is modelled in finite element method and water jet in Smooth Particle Hydrodynamics. SPH is preffered to overcome mesh tangling in extreme deformation conditions. While there is no grid in SPH method particles become as computational framework.

- Johnson and Cook Model

Interaction of solid missile and fluid water is calculated using Johnson and Cook Plasticity Model in Ls-Dyna. The flow stress is given with:

$$\sigma_y = (A+B\epsilon^{-p^n})(1+c\ln\dot{\epsilon})(1-T^m) \quad (1)$$

A,B,C and n are $1.67.10^8$, $5.96.10^8$, 0.001 and 0.051 respectively. Temperature effects and m are neglected.

ϵ^{-p} = effective plastic strain (2)

$$\dot{\epsilon} = \frac{\dot{\epsilon}^{-p}}{\dot{\epsilon}_0} \quad (3)$$

Effective plastic strain rate for $\dot{\epsilon}_0$ in units of 1/time.

$$T = \frac{T - Tenv}{Tmelt - Tenv} \quad (4)$$

Temperature difference is neglected in this study.

When there is a flow stress on plastic strain there is nonlinearity. Increment in plastic strain is calculated by iterations however using Taylor series expansion with linearization due to current time enables solving equation sufficiently accurate enough.

$$\epsilon^{f} = [D_1 + D_2 \exp(D_3\sigma)][1 + D_4 ln\epsilon][1 + D_5 T] \qquad (6)$$

Di i= 1,…..,5 are 0.0261, 0.0263, -0.349, 0.247 and 16.799 respectively. σ is the ratio of pressure divided by effective stress.

$$\sigma = \frac{p}{\sigma_{eff}} \qquad (7)$$

Fracture occurs when damage parameter reaches 1.

$$D_p = \Sigma \frac{\Delta\epsilon^{-p}}{\epsilon f} \qquad (8)$$

- Gruniesen Model

Equation of state for pressure velocity particle for compressed materials is given with Gruniesen in LS-Dyna.

$$p = \frac{\rho_0 c^2 \mu[1+\left(1-\frac{\Upsilon_0}{2}\right)\mu-\frac{a}{2}\mu^2]}{[1-(S_1-1)\mu-S_2\frac{\mu^2}{\mu+1}-S_3\frac{\mu^3}{(\mu+1)^2}]^2} + (\Upsilon_0 + \alpha\mu)E_v \qquad (1)$$

E is internal energy per volüme, C is the intercept of the µs -µp curve, S_1, $S_2$and $S_3$are the coefficients of the slope of the µs -µp curve, Υ_0 is the Gruniesen gamma, and a is the first order volüme correction to Υ_0. Constants C, S_1, S_2, S_3, Υ_0 and a are input parameters defined as 1647, 1.921, -0.096, 0 and 0.35 respectively. The compression is defined in terms of the relative volüme, V, as;

$$\mu = \frac{1}{v} - 1 \qquad (2)$$

For expanded materials the pressure is defined by:

$$p=\rho_0 c^2\ \mu + \ (\Upsilon_0 + \alpha\mu)E \qquad (3)$$

On the other hand when internal energy per initial volüme is linear, E is given with a polynomial equation which is also linear in form.

$$p=C_0+ C_1\mu + C_2\mu^2 + C_3\mu^3 + (C_4 + C_5\mu + C_6\mu^2)E \qquad (4)$$

Here $C_0, C_1, C_2, C_3, C_4,$ C_5 and C_6 are constants and C_0=-1.00E5 for air and C_1=6.80E10 for aluminum and other constants are zero.

$\mu = \frac{1}{v} - 1$ (5)

where V is the relative volüme. In expanded elements, the coefficients of μ^2 are set to zero.

Missile material is in finite elements and water jet is in SPH mode. These two is coupled with contact algorithms where finite elements is defined as master and SPH elements is defined as slave parts.

The SPH method is based on a quadrature formula for moving particles $((\mathbf{x}_i(t))\ i \in \{1..N\}$, where $\mathbf{x}_i(t)$ is the location of particle i, which moves along the velocity field v. The particle approximation of a function can now be defined by:

$$\Pi^h f\,(\mathbf{x}_i) = \sum_{i=1}^{N} w_j f(\mathbf{x}_i) W(\mathbf{x}_i - \mathbf{x}_j, h) \quad (6)$$

where $w_j = m_j/\rho_j$ is the "weight" of the particle. The weight of a particle varies proportionally to the divergence of the flow.

The SPH formalism implies a derivative operator. A particle approximation for the derivative operator must be defined. Gradient of a function is defined as

$$\nabla f\,(x) = \nabla f\,(x) - f\,(x)\nabla 1(x) \quad (7)$$

where 1 is the unit function. Starting from this relation, the particle approximation to the gradient of a function is given with:

$$\Pi^h \nabla f\,(\mathbf{x}_i) = \sum_{j=1}^{N} \frac{m_j}{\rho_j}[f\,(\mathbf{x}_j)A_{ij} - f\,(\mathbf{x}_i)A_{ij}] \quad (8)$$

where

$$A_{ij} = \frac{1}{h^{d+1}}\theta'(||\mathbf{x}_i - \mathbf{x}_j||)\frac{1}{h} \quad (9)$$

The particle approximation of the partial derivative $\partial/\partial x^\alpha$ is defined as:

$$\Pi^h(\partial f \frac{\partial \mathrm{f}}{\partial \mathrm{x}^\alpha})(\mathbf{x}_i) = \sum_{j=1}^{N} w_j\, f(\mathbf{x}_j A^\alpha(\mathbf{x}_i, \mathbf{x}_j) \quad (10)$$

where **A** is the operator defined by:

$$\mathbf{A}(\mathbf{x}_i, \mathbf{x}_j) = \frac{1}{h^{d+1}(x_i,x_j)} \frac{(\mathrm{xi-xj})}{||\mathrm{xi-xj}||} \theta'\left(\frac{||\mathrm{xi-xj}||}{(\mathrm{h(xi,xj)})}\right) \quad (11)$$

A^α is the component α of the **A** vector.

Strong formulation is not conservative in SPH methods so weak formulation approximation is is used to solve conservative equations encountered in SPH.

The weak formulation approximation: The adjoint of the Lv operator is used:

$$Lv : \phi \rightarrow Lv\ (\phi) = \partial\phi/\partial t + \sum_{l=1}^{d} v^l \frac{\partial \phi}{\partial x^l} \quad (12)$$

The discrete form of this operator corresponds to the discrete formulation of the adjoint of Dh,s:

$$Dh,s\ \phi(\mathbf{x}_i) = \sum_{j=1}^{N} w_j (\phi(\mathbf{x}_i) A_{ij} - \phi(\mathbf{x}_j) A_{ji}) \quad (13)$$

A discrete adjoint operator for the partial derivative is also defined, and is taken to be the $\alpha{-}th$ component of the operator

$$D_\alpha \phi(\mathbf{x}_i) = \sum_{j=1}^{N} w_j \phi(\mathbf{x}_i) A^\alpha(\mathrm{x_i,x_j}) - \mathrm{w_j} \phi(\mathbf{x}\mathrm{i})\ A^\alpha(\mathrm{x_j,x_i}) \quad (14)$$

- Applications to Conservation Equations

The conservation equations are written in their discrete form.

Momentum conservation equation:

$$\frac{dv^\alpha}{dt}(\mathbf{x}_i(t)) = (1/\rho_i) \frac{\partial(\sigma^{\alpha\beta})}{\partial \mathrm{x}_i})(\mathbf{x}_i(t)) \quad (1)$$

where α, β are the space indices.

The particle approximation of the weak form of this equation is:

$$\frac{dv^\alpha}{dt}(\mathbf{x}_i) = \sum_{j=1}^{N} m_j \left(\frac{\sigma^{\alpha,\beta}(x_i)}{\rho_i{}^2} A_{ij} - \frac{\sigma^{\alpha,\beta}(x_j)}{\rho_j{}^2} A_{ji}\right) \quad (2)$$

Energy conservation equation:

$$dE/dt = -\frac{p}{\rho} \nabla \mathbf{v} \quad (3)$$

The particle approximation equation is:

$$\frac{dE}{dt}(\mathrm{x_i}) = -\frac{p_i}{\rho_i{}^2} \sum_{j=1}^{N} m_j (\mathrm{v(x_j)} - \mathrm{v(x_i)}) \mathrm{A_{ij}} \quad (4)$$

- Time Step Control

During the simulation, to update the stresses and the right hand side force vector solutions are looped through the elemets.

Taking the minimum value over all elements a new time step is determined with:

$\Delta t^{n+1} = a \cdot \min\{\Delta t1, \Delta t2, \Delta t3, \ldots, \Delta tN\}$ (1)

where N is the number of elements which is 18561.

For stability reasons the scale factor a is typically set to a value of 0.9 (default) or some smaller value. In this study 0.45 is set for scale factor.

- Hourglass control

Oscillation modes of solid particles which are also called zero energy modes is evaluated by Hourglass Control mode in Ls-Dyna. These oscillations are undesirable if the frequency is higher compared to structural response. On the other hand if frequency is closer to structural response it must be accounted. Hourglass control adjusts the frequency modes using damping elements stopping anomalies but negligible effect on normal frequency modes.

- Pressure Boundary Conditions is given with the formula

$\int_{\partial b1} N^t t ds$ (1)

a Gaussian quadrature rule is used. To locate any point of the surface under consideration, a position vector, r, is defined:

$r = f1(\xi, \eta)i1 + f2((\xi, \eta)i2 + f3(\xi, \eta)i3$ (2)

where

$fi(\xi, \eta) = \sum_{j=1}^{4} \phi_j x_i{}^j$ (3)

and $i1$, $i2$, $i3$ are unit vectors in the $x1$, $x2$, $x3$ directions. Nodal quantities are interpolated over the four-node linear surface by the functions

$\phi i = \frac{1}{4}(1+\xi\xi i)(1 + \eta\eta i)$ (4)

so that the differential surface area ds may be written in terms of the curvilinear coordinates as

$ds = |J| d\xi d\eta$ (5)

where $|J|$ is the surface Jacobian defined by

$|J| = \left| \frac{\partial r}{\partial \xi} \times \frac{\partial r}{\partial \eta} \right| = (EG - F2)0.5$ (6)

in which

$$E = \frac{\partial r}{\partial \xi} \cdot \frac{\partial r}{\partial \xi}, \quad (7)$$

$$F = \frac{\partial r}{\partial \xi} \cdot \frac{\partial r}{\partial \eta}, \quad (8)$$

$$G = \frac{\partial r}{\partial \eta} \cdot \frac{\partial r}{\partial \eta}, \quad (9)$$

A unit normal vector **n** to the surface segment is given by

$$\mathbf{n} = |J|-1 \left(\frac{\partial r}{\partial \xi} \times \frac{\partial r}{\partial \eta}\right) \quad (10)$$

and the global components of the traction vector is written as;

$$ti = ni \sum_{j=1}^{4} \phi_j p^j \quad (11)$$

where pj is the applied pressure at the jth node.

The surface integral for a segment is evaluated as:

$$\iint_{-1}^{1} \mathrm{Nt}\ \mathrm{t}|\mathrm{J}|\mathrm{d}\xi\ \mathrm{d}\eta \quad (12)$$

One such integral is computed for each surface segment on which a pressure loading acts.

3.3. Water Jet Properties

Water jet is assumed to be in continuous flow and not pulsative so erosion quantity according to impact number and fatigue process is neglected. Pressure exceeding the yield strength of missile material, force to divert or detonate the missile is investigated by this point of view.

In order to get the same results using high pressure water jets;

1. Momentum of water jet directly hitting missile in horizontal axis deforming the shape of warhead
2. Hydraulic penetration due to stress on warhead material exposed to high pressure water jet disrupting missile explosion trigger system
3. Diverting missile before hitting the target vehicle with high speed velocity jet's momentum. After 1.68D it is assumed that WJ loses its force and momentum affects.

In order to achieve results nozul diameter, jet velocity and stand off distances are varied changed and examined. Model geometry is given in Figure 3.1.

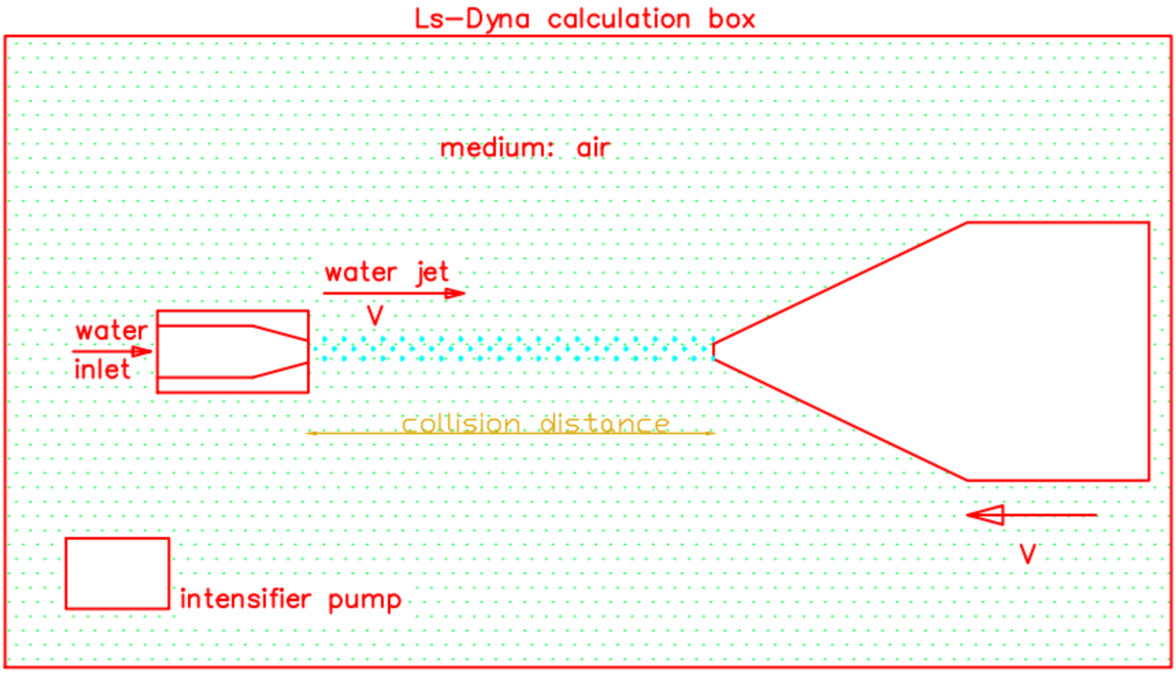

Figure 3.1. Model Geometry

3.4. Simulation Preparation - LS-Dyna / Ls Prepost

Model of an aluminium missile warhead is drawn and meshed in LS-Prepost. Air and water media is first prepared as planar surfaces. Then using LS-Prepost surface of both media planar mesh size is identified. In the next step using Element generation planar surfaces are extruded and 3D forms are given. After formation the last mesh size are defined for both air and water.

Using Smooth Partical Hydrodynamics (SPH) 3D form of air and water are transferred into fluid particles with appropriate density.

For related nozzle diameter, water jet speed, air length and the distance of collision LS-Prepost keyword files are prepared. Related simulation parameter variation is given in Table 3.1. Keyword files are used in LS-Dyna processor to run the simulations. Simulation parameters are based on nozzle diameter, water jet velocity and collision distance from jet spray. Water and air interaction is shown in Figure 3.2.

Table 3.1. Simulation Parameter Variation

Constants			Variable
No	Nozzle Diameter - mm	Velocity - m/s	Graph
1	2	150	Collision Point
2	4	500	Collision Point
3	6	500	Collision Point
4	10	500	Collision Point
No	Nozzle Diameter - mm	Collision Point - mm	Graph
5	2	300	Velocity
6	4	300	Velocity
7	6	300	Velocity
8	10	600	Velocity
No	Velocity - m/s	Collision Point - mm	Graph
9	150	300	Nozzle Diameter
10	500	300	Nozzle Diameter
11	500	600	Nozzle Diameter

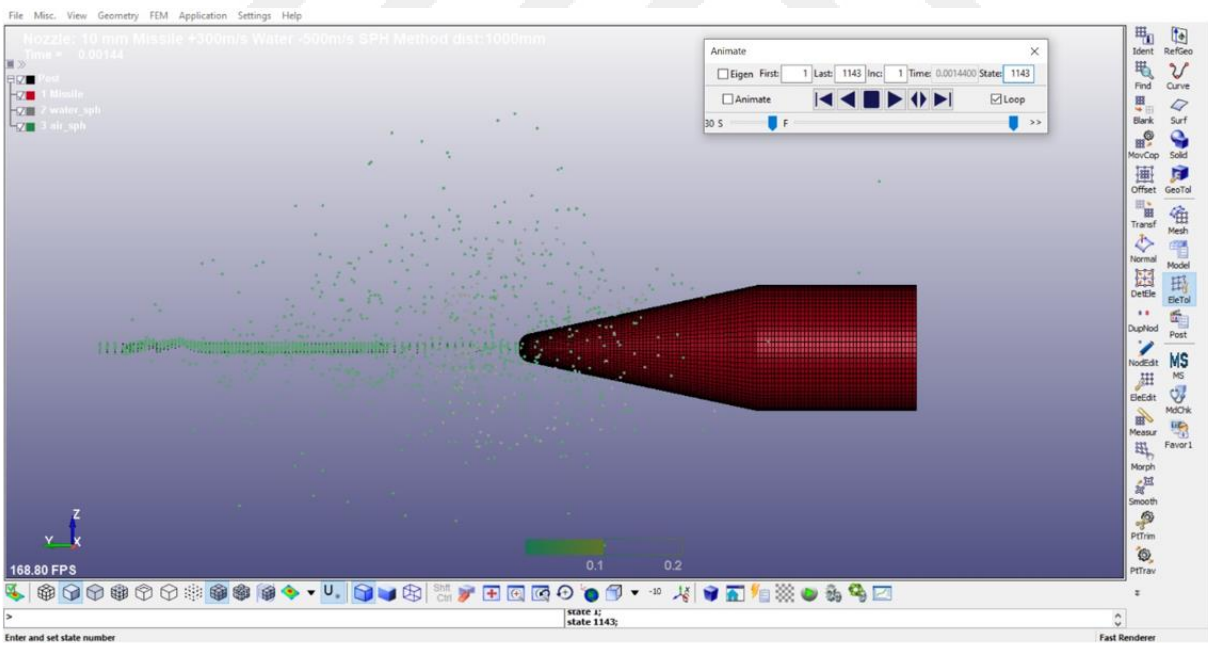

Figure 3.2. Air and WJ interaction. D:10mm WJ: 500 m/s Distance:1000mm

4. RESULTS AND DISCUSSIONS

Numerical results of this study were taken in this section for 3 parameters in 3 divisions and 13 simulations. Nozzle diameter, WJ velocity and collision distance are varied, and individual affects of each parameter is evaluated for WJ on missile. Besides for different contact angles deflection of missile from target point is investigated. Relevant impuls and resultant momentum graphics are given due to nozzle diameter, collision distance and WJ velocity relation as figures, after explanation of related simulation groups. In Table 4.1. results are summarized.

a) Variable Collision Point – Constant Nozzle Diameter and Water Jet Velocity:

Nozzle diamaters and WJ velocity are constant in 1,2,5,6,7,9,10,11, and 13th simulations. Resultant momentum and impuls values were evaluated due to collision distance change.

b) Variable WJ Velocity – Constant Nozzle Diameter and Collision Distance:

Nozzle diameter and distance are constant in 2,3,4,5,8,9,11, and 12th simulations. Resultant momentum and impuls values were evaluated due to water jet velocity change.

c) Variable Nozzle Diameter – Constant Water Jet Velocity and Collision Distance:

WJ velocity and distance are constant in 2,3,4,5,7,8,9,10 and 11th simulations. Resultant momentum and impuls values were evaluated due to nozzle diameter dimension.

4.1. Effect of Collision Distance on Missile Motion

In simulations 1 and 2, nozzle diameter is 2 mm and WJ velocity is set 150 m/s. Missile and WJ interaction distance is arranged for 200 and 300 mm to investigate the effect of distance increase in missile resultant momentum caused by high velocity WJ impact. No significant change was observed is R-M whereas there is a 37.83% increase in impuls. This may be caused of subsonic flow where coherent length may be longer.

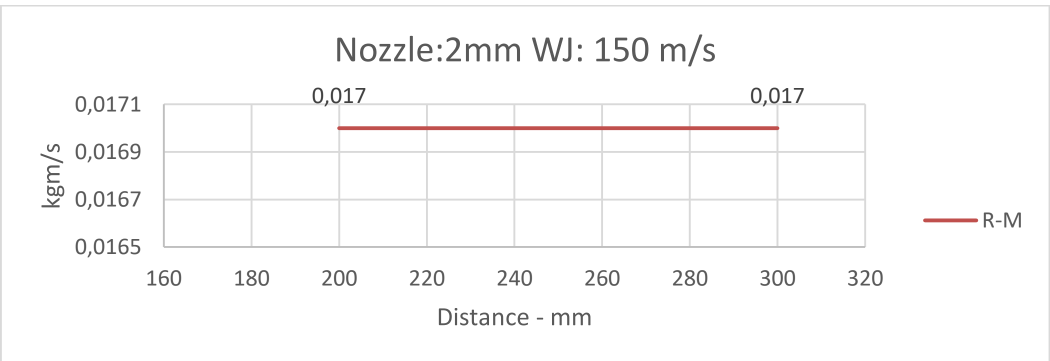

Figure 4.1. Resultant Momentum vs Distance D:2 mm WJ: 150 m/s

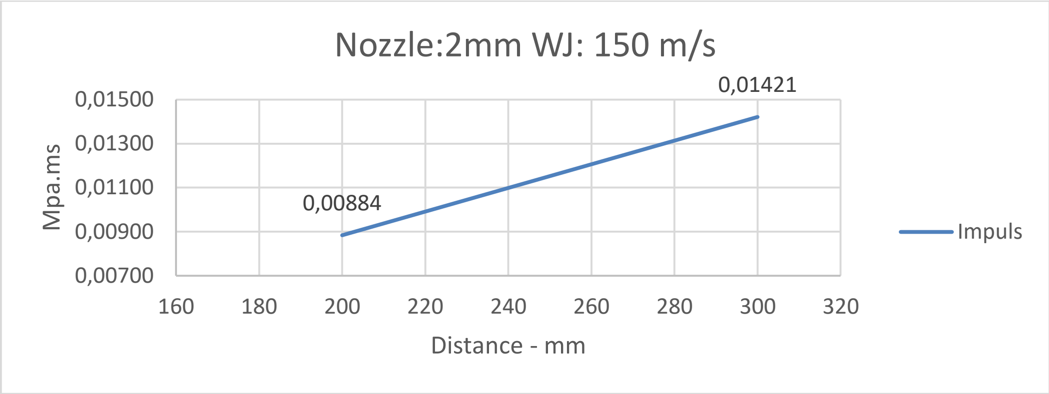

Figure 4.2. Impuls vs Distance. D:2 mm WJ: 150 m/s

In simulations 5,6 and 7, nozzle diameter is 4 mm and WJ velocity is set 500 m/s. Missile and WJ interaction distance is arranged between 300 and 600 mm. In the coherent zone limit -was 100D as mentioned before- at 400 mm, maximum R-M and impuls values are observed. R-M increased 23.38% and impuls increased 36.98% in 300 – 400 mm region.

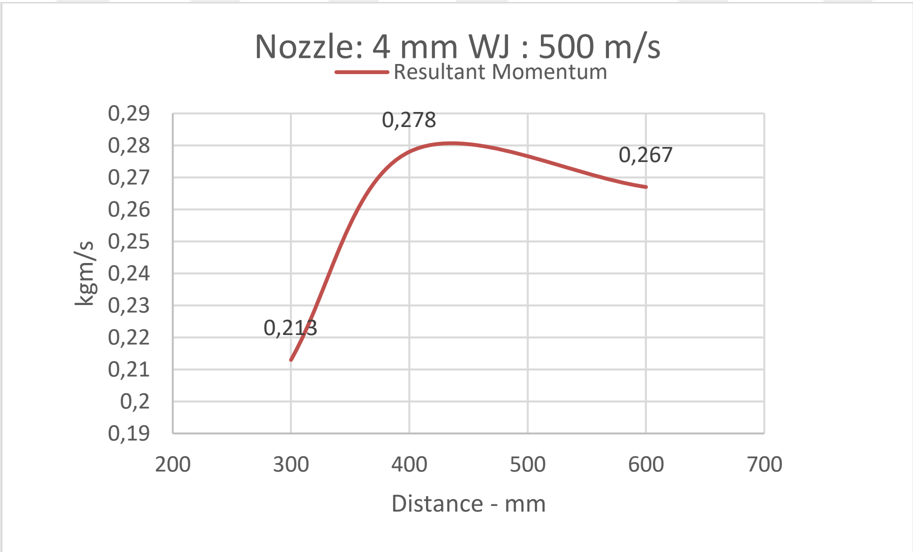

Figure 4.3. Resultant Momentum vs Distance. D: 4 mm WJ:500m/s

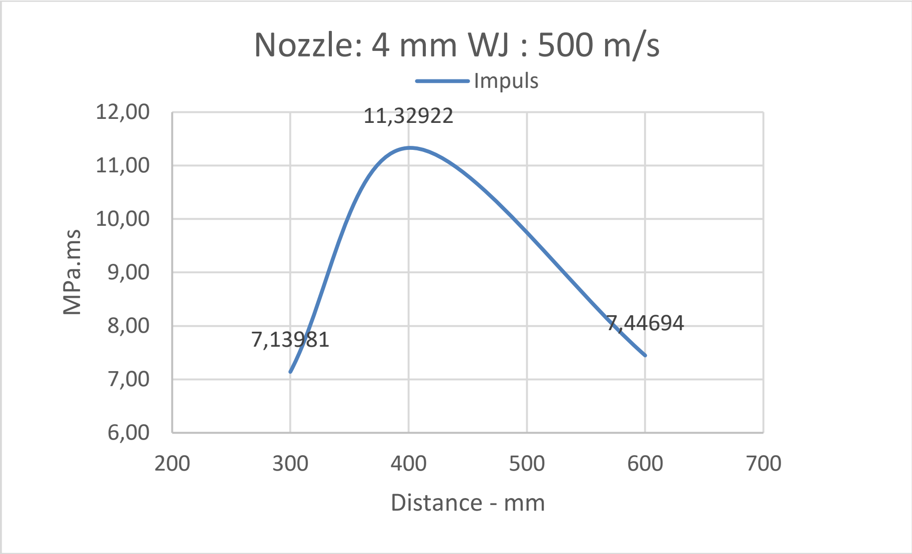

Figure 4.4. Impuls vs Distance. D: 4 mm WJ:500m/s

In simulations 9 and 10, nozzle diameter is 6 mm and WJ velocity is set 500 m/s. Missile and WJ interaction distance is arranged between 300 and 600 mm. At coherent zone limit, which is 600 mm, maximum R-M and impuls values are observed. R-M increased 58.44% and impuls increased 25.23 % in 300 – 600 mm region.

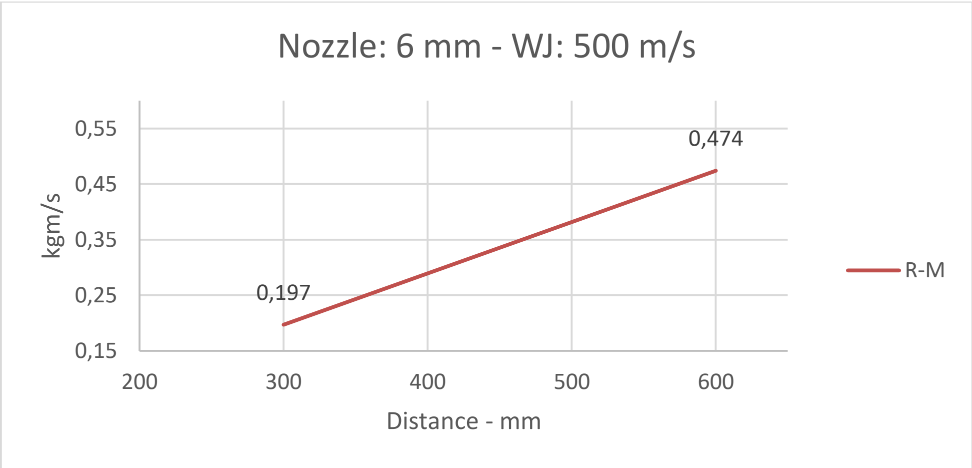

Figure 4.5. Resultant Momentum vs Distance. D: 6 mm WJ:500m/s

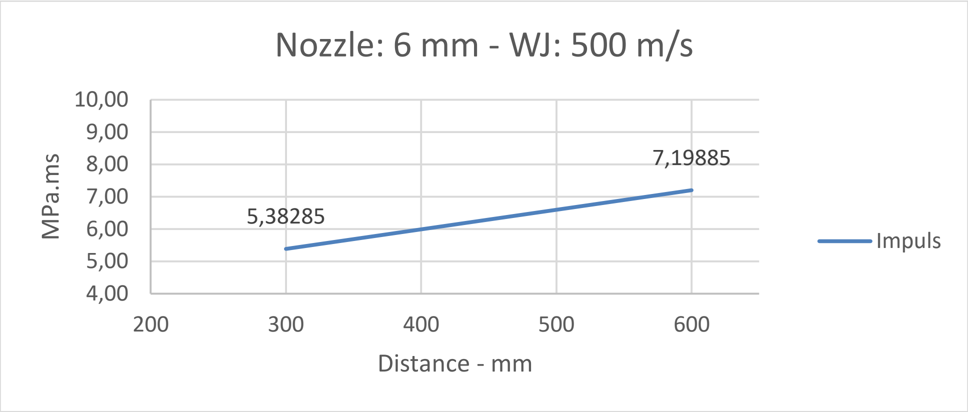

Figure 4.6. Impuls vs Distance. D:6 mm WJ: 500 m/s

In simulations 11 and 13, nozzle diameter is 10 mm and WJ velocity is set 500 m/s. Missile and WJ interaction distance is arranged between 600 and 1000 mm. Unlike 4- and 6-mm nozzles spraying jet at same velocity, 10 mm nozzle has its maximum, not at coherent zone limit but at 600 mm. R-M decreased from 0.798 to 0.77 kgm/s and impuls decreased from 6.14 to 4.44 MPa.ms when distance is increased from 600 to 1000 mm. Decreases of 3.51% in R-M and 27.61 % in impuls is considered to be related with high We number of 10 mm nozzle because it has bigger droplet size and characteristic length compared to 4 an 6 mm nozzles.

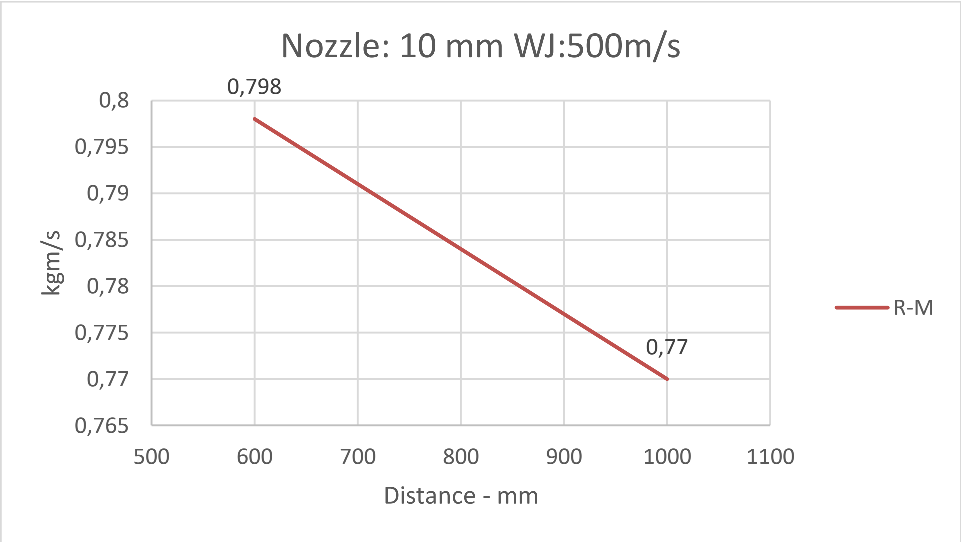

Figure 4.7. Resultant Momentum vs Distance. D:10 mm WJ: 500 m/s

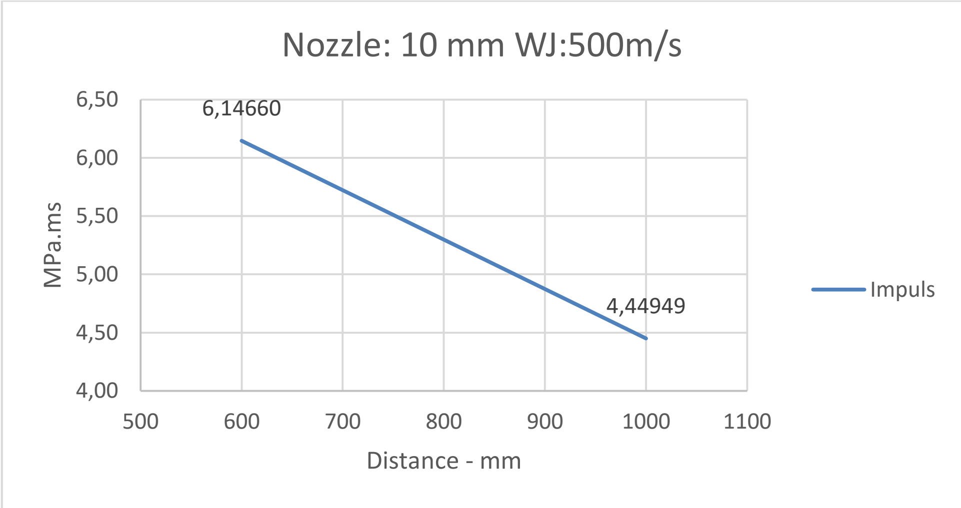

Figure 4.8. Impuls vs Distance. D:10 mm WJ: 500 m/s

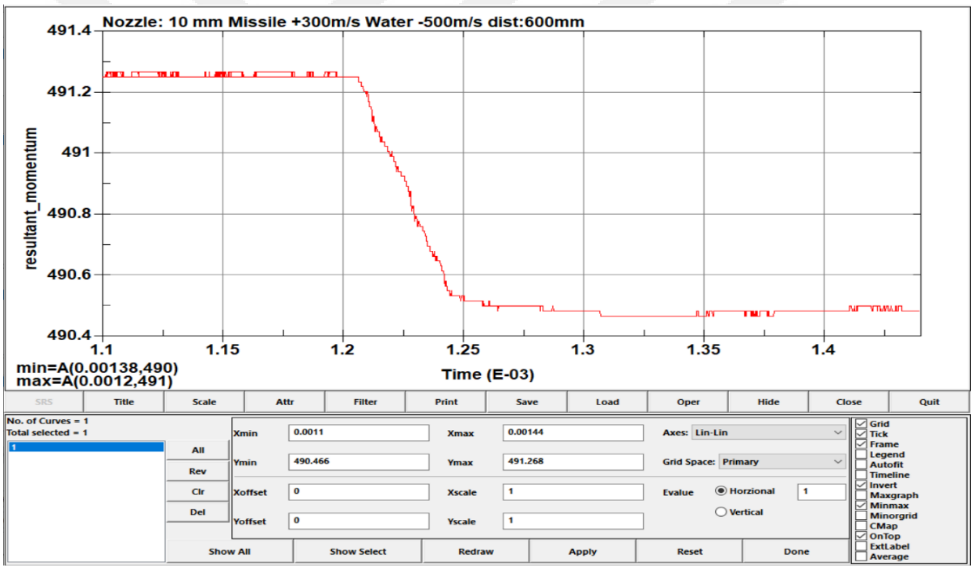

Figure 4.9. Resultant moment change D: 10 mm WJ: 500 m/s Dist: 600mm

4.2. Effect of WJ Velocity on Missile Motion

In simulations 2 and 3, nozzle diameter is 2 mm and collision distance is set at 300 mm. WJ velocity changes between 150 and 500 m/s. R-M results did not change. Impuls values cannot be determined. 300 mm range is out of coherent zone for 2 mm nozzle which is 200m. Beyond this distance water jet may have no impuls affect on missile motion related with high We number.

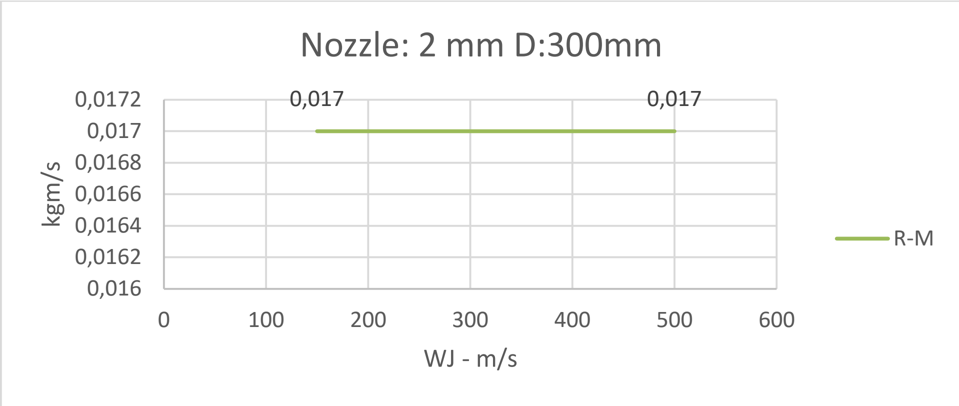

Figure 4.10. Resultant Momentum vs WJ Velocity. D:2mm Dist:300mm

In simulations 4 and 5, nozzle diameter is 4 mm and collision distance is set at 300 mm. WJ velocity changes between 150 and 500 m/s. R-M value decreased by a value of 6.99% and impuls decreased 1.15%. 2^{nd} power of velocity in We formula is considered to be the reason of this adverse effect because interaction takes place in coherent zone and increasing values are expected directly proportional to velocity. Defined coherent zone for high speed flows may be shorter for supersonic flow.

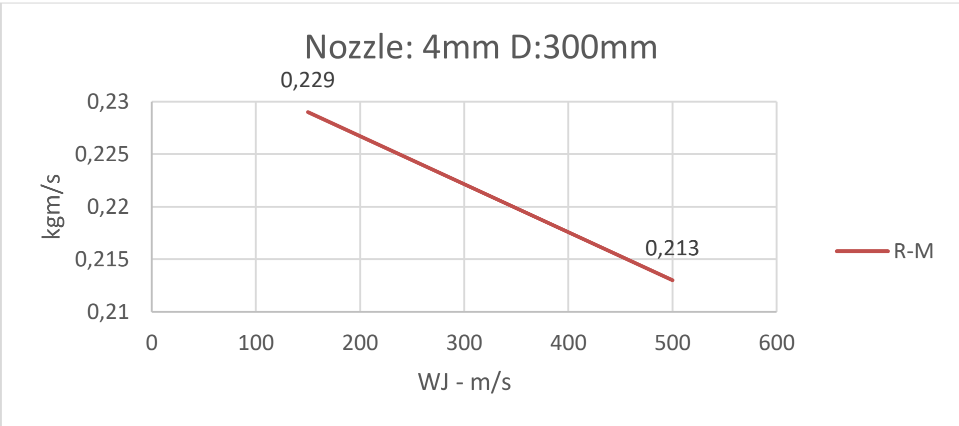

Figure 4.11. Resultant Momentum vs WJ Velocity. D:4mm Dist:300mm

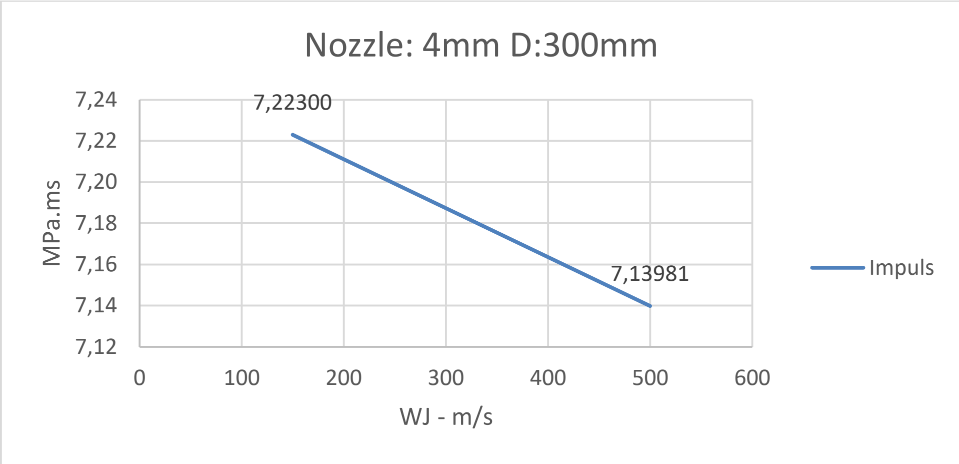

Figure 4.12. Impuls vs WJ Velocity. D:4mm Dist:300mm

In simulations 8 and 9, nozzle diameter is 6 mm and collision distance is set at 300 mm. WJ velocity changes between 150 and 500 m/s. R-M value increased by a value of 67.51% and impuls increased 17.17%.

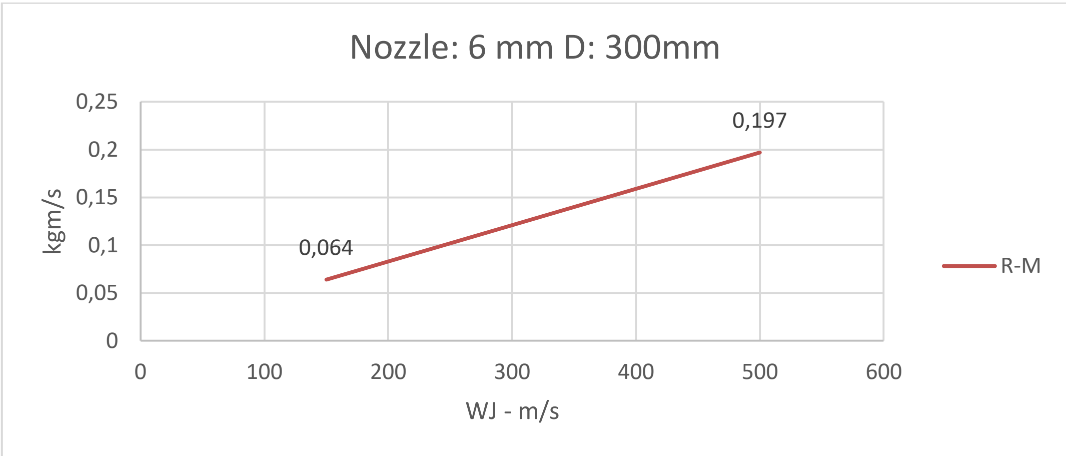

Figure 4.13. Resultant Momentum vs WJ Velocity. D:6mm Dist:300mm

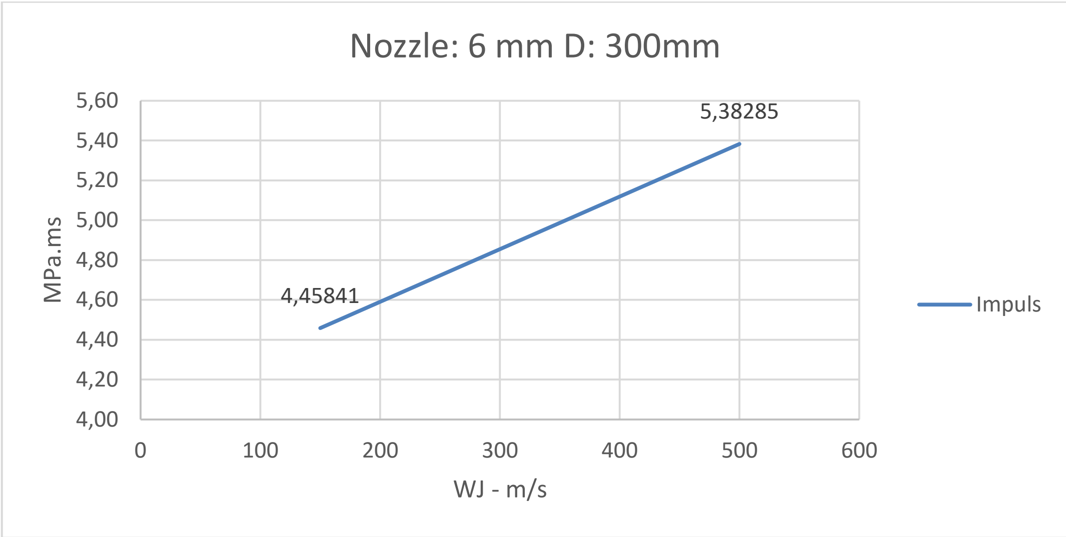

Figure 4.14. Impuls vs WJ Velocity. D:6mm Dist:300mm

In simulations 11 and 12, nozzle diameter is 10 mm and collision distance is set at 600 mm. WJ velocity changes between 150 and 500 m/s. R-M value increased by a value of 59.02% and impuls increased 58.60%.

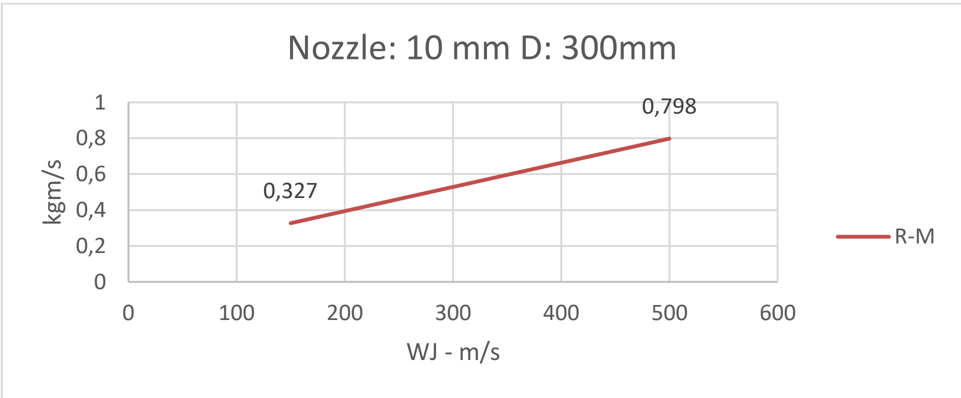

Figure 4.15. Resultant Momentum vs WJ Velocity. D:10 mm Dist:300mm

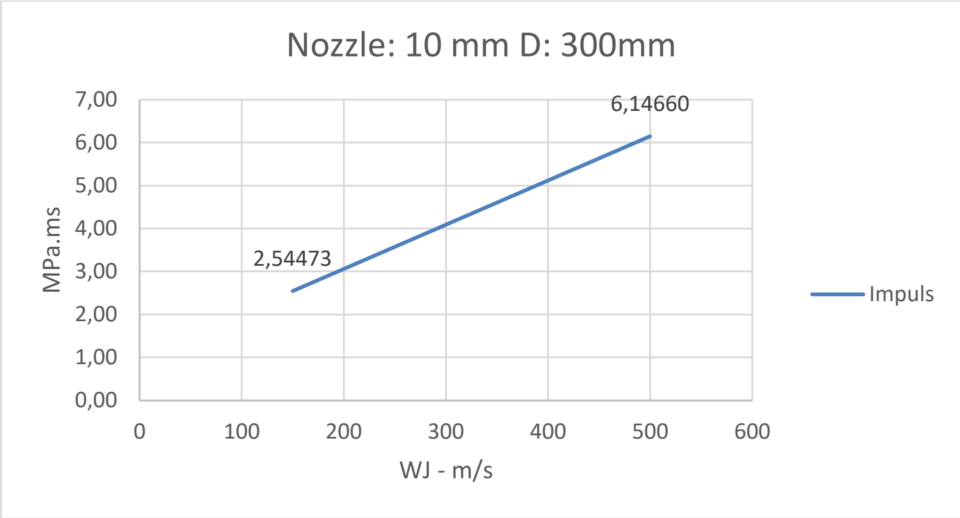

Figure 4.16. Impuls vs WJ Velocity. D:10mm Dist:300mm

4.3. Effect of Nozzle Diameter on Missile Motion

In simulations 2,4 and 8, collision distance is 300 mm and WJ velocity is set at 150 m/s. Nozzle diameters are 2,4- and 6-mm. Highest R-M and impuls values are read for 4 mm nozzle which are 0.229 kgm/s and 7.22 MPa.ms respectively. On the 2 mm nozzle side of the graph R-M decreases 92.58% and impuls decreases 99.8 %. On the 6 mm side R-M decreases 72.05% and impuls decreases 38.27 %. The radial effect area of water jet and missile radome geometry interaction can cause these results because normally 6 mm is expected to have higher R-M and impuls values. Most efficient nozzle type at this velocity and range is 4mm.

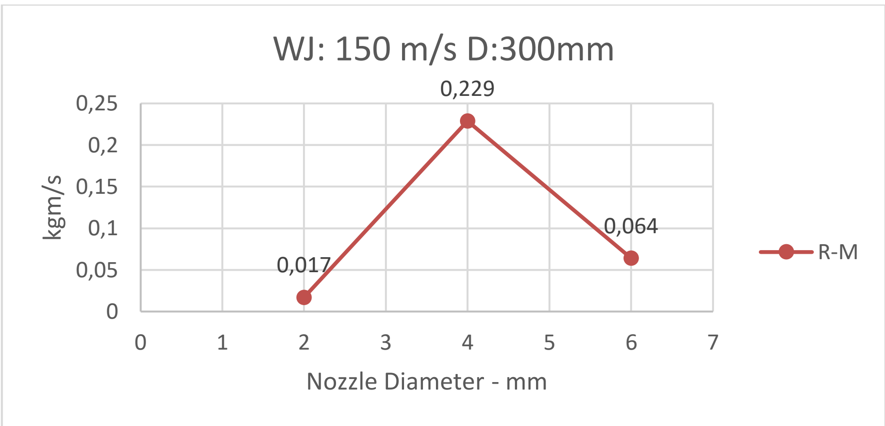

Figure 4.17. Resultant Momentum vs Nozzle Diameter. WJ: 150 m/s Dist:300mm

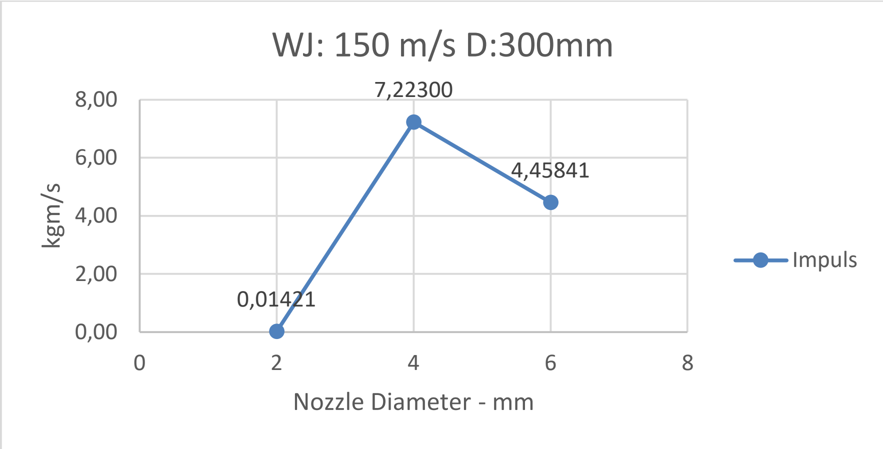

Figure 4.18. Impuls vs Nozzle Diameter. WJ: 150 m/s Dist:300mm

In simulations 3,5 and 9, collision distance is 300 mm and WJ velocity is set at 500 m/s. Nozzle diameters are 2,4- and 6-mm. Highest R-M and impuls values are read again for 4 mm nozzle which are 0.213 kgm/s and 7.13 MPa.ms respectively. On the 2 mm nozzle side of the graph R-M decreases 92.02%. Impuls can not be determined. On the 6 mm side R-M decreases 7.51% and impuls decreases 24.60 %. Like simulations 2,4 and 8 of nozzle group, these results are tought to be sourced from missile radome interaction.

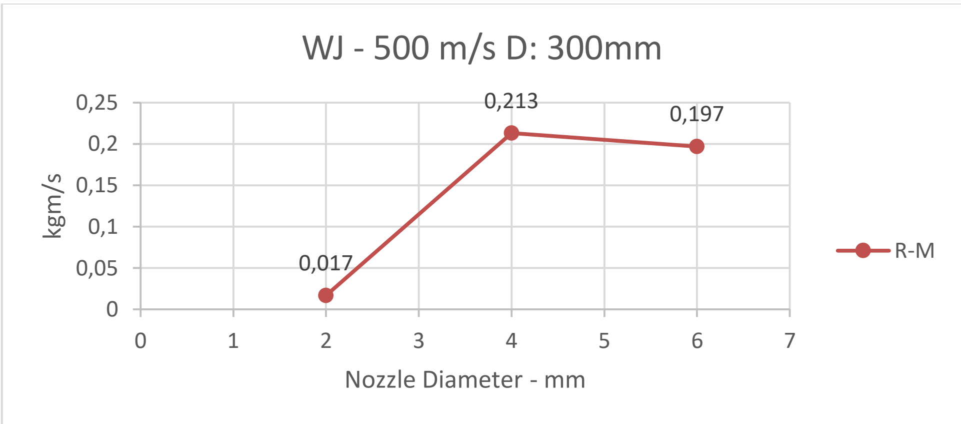

Figure 4.19. Resultant Momentum vs Nozzle Diameter. WJ: 500 m/s Dist:300mm

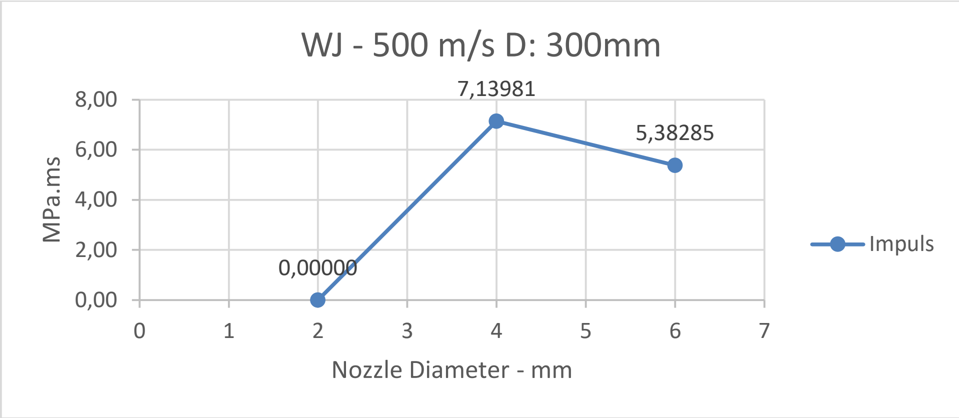

Figure 4.20. Impuls vs Nozzle Diameter. WJ: 500 m/s Dist:300mm

In simulations 7,10 and 11, collision distance is 600 mm and WJ velocity is set at 500 m/s. Nozzle diameters are 4,6- and 10-mm. Highest R-M and minimum impuls values are read for 10 mm nozzle which are 0.798 kgm/s and 6.14 MPa.ms respectively. Increasing nozzle diameter effects bigger areas on missile radome so decrease in impuls values are similar to other results on the other hand in coherent zone of 10 mm nozzle increase in R-m values are observed.

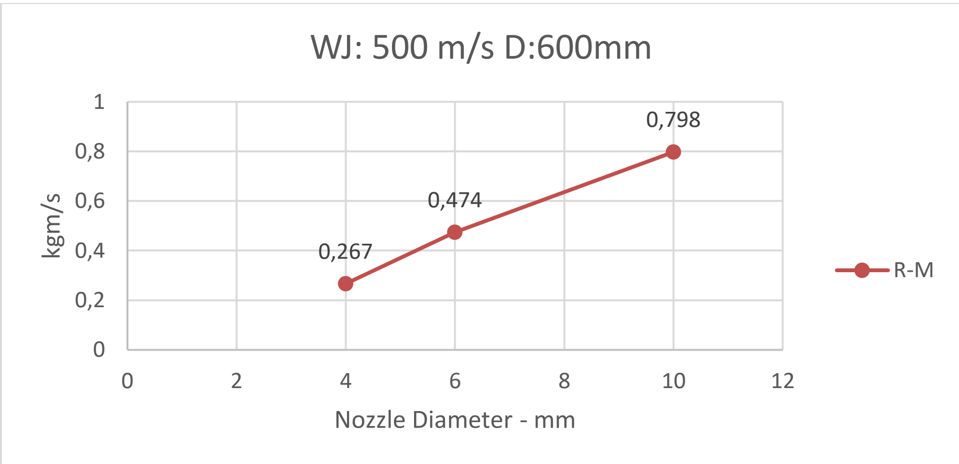

Figure 4.21. Resultant Momentum vs Nozzle Diameter. WJ: 500 m/s Dist:600mm

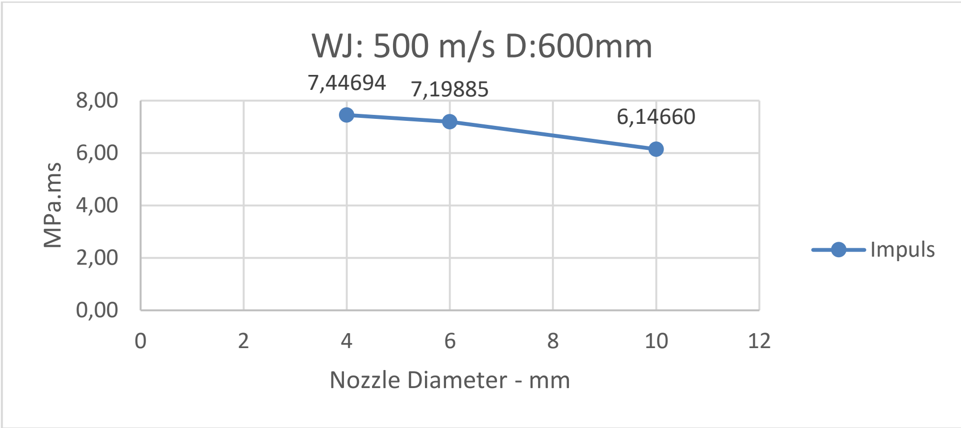

Figure 4.22. Impuls vs Nozzle Diameter. WJ: 500 m/s Dist:600mm

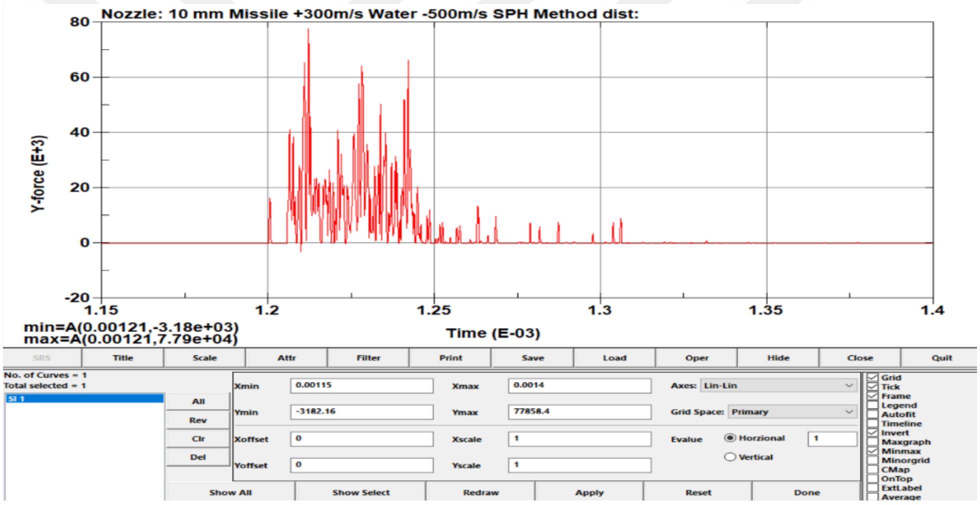

Figure 4.23. Y-component of force due to time. D:10mm WJ: 500 m/s. Dist: 600 mm

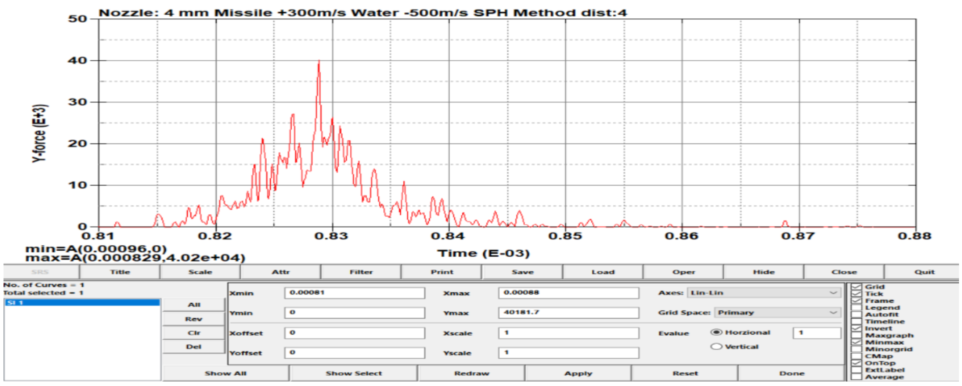

Figure 4.24. Y-component of force due to time. D:4mm WJ: 500 m/s. Dist: 400 mm

Table 4.1. Simulation Results Summary

No	1	2	3	4	5	6	7	8	9	10	11	12	13
Nozzle Diameter - mm	2	2	2	4	4	4	4	6	6	6	10	10	10
WJ Velocity - m/s	150	150	500	150	500	500	500	150	500	500	500	150	500
Missile Velocity - m/s	300	300	300	300	300	300	300	300	300	300	300	300	300
Collision Distance - mm	200	300	300	300	300	400	600	300	300	600	600	600	1000
Von Mises Stress - Mpa	0.66	0.69	0.74	127	124	121.5	93.29	151	175.4	185.6	387.4	156	213
Effective Plastic Strain	ND	ND	ND	0.028	0.076	0.071	0.012	0.073	0.12	0.19	0.47	0.17	0.333
Resultant Momentum - kgm/s	0.017	0.017	0.017	0.229	0.213	0.278	0.267	0.064	0.197	0.474	0.798	0.327	0.77
Pressure - Mpa	0.44	0.36	0.29	65.07	86.44	86.27	40.65	83.17	62.6	71	109.5	83.63	129.7
Deformation - mm	ND	ND	ND	0.126	0.449	0.326	0.029	0.112	0.571	1.022	2.8	1.642	0.884
Force - N	195.85	360	ND	13847.6	40516.8	40181.7	17608.2	15812.8	57274.6	45958.3	77858.4	22563.7	49316.1
Average Time - Δt - ms	0.0008	0.0007	ND	0.037	0.0125	0.02	0.03	0.045	0.015	0.025	0.035	0.05	0.04
Calculated Impuls - (F.Δt) N.ms	0.08	0.13	ND	256.18	253.23	401.82	264.12	355.79	429.56	574.48	1362.52	564.09	986.32
Affected Area - mm2	8.87	8.87	8.87	35.47	35.47	35.47	35.47	79.80	79.80	79.80	221.67	221.67	221.67
Impuls - MPa.ms	0.00884	0.01421	ND	7.22300	7.13981	11.32922	7.44694	4.45841	5.38285	7.19885	6.14660	2.54473	4.44949

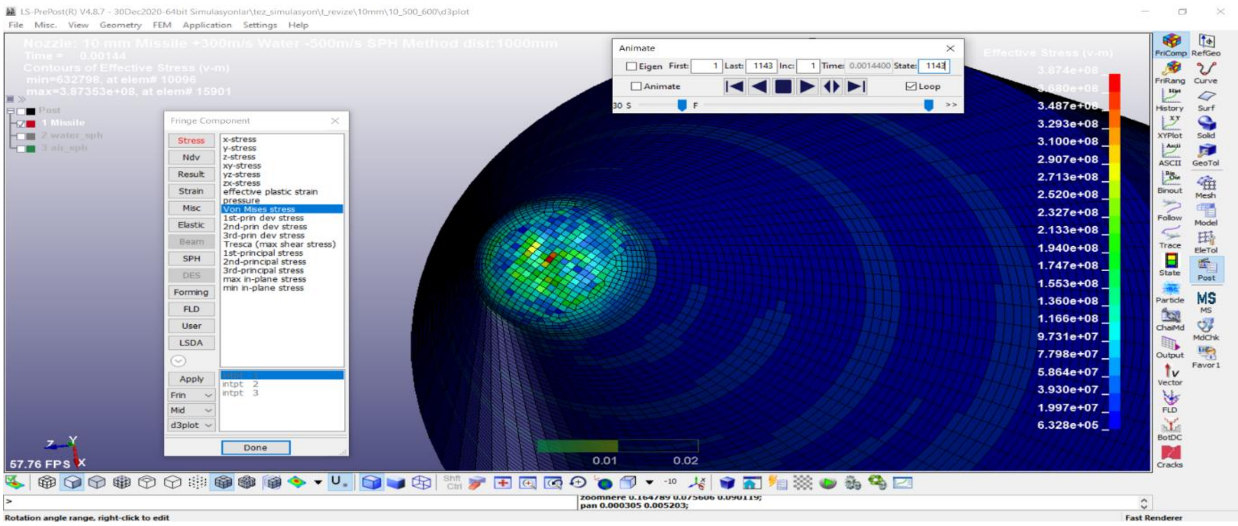

Figure 4.25. Effective stress (v-m) observed on missile radome. D:10mm WJ: 500 m/s Distance:600mm. Radome deformation process also observed.

4.4. Missile Diverting and Deactivating

Water jet and missile interaction is studied for 30^0, 45^0 and 60^0 contact angles. It is briefly illustrated in Figure 4.26. Distance between WJ and missile is assumed to be equal to collision distance. Relevant distance between target and missile is calculated due to interaction angle. Simulation results are used as a source for force and time needed in calculations and results are given in Table 4.2. Especially HEAT type warheads' spear like molten formation effects can be reduced using water jets this way and armored vehicle can be protected.

Table 4.2. Deflection Results Due to AoC

Nozzle Diameter - mm	4	4	4	4	6	6	6	10	10	10
Force - N	13847.6	40516.8	40181.7	17608.2	15812.8	57274.6	45958.3	77858.4	22563.7	49316.1
WJ Velocity - m/s	150	500	500	500	150	500	500	500	150	500
Missile-Target distance for 30° AoC	258	258	344	516	258	258	516	516	516	860
Missile-Target distance for 45° AoC	212.1	212.1	282.8	424.2	212.1	212.1	424.2	424.2	424.2	707
Missile-Target distance for 60° AoC	150	150	200	300	150	150	300	300	300	500
Collision Distance - mm	300	300	400	600	300	300	600	600	600	1000
Missile Velocity - m/s	300	300	300	300	300	300	300	300	300	300
Deflection at 30° mm	2.60	7.88	14.13	13.61	2.98	11.39	38.26	70.81	17.66	126.15
Deflection at 45° mm	2.48	7.41	13.20	12.82	2.83	10.62	35.10	62.77	16.56	111.26
Deflection at 60° mm	1.50	4.43	7.85	7.68	1.71	6.30	20.52	35.63	9.88	62.90

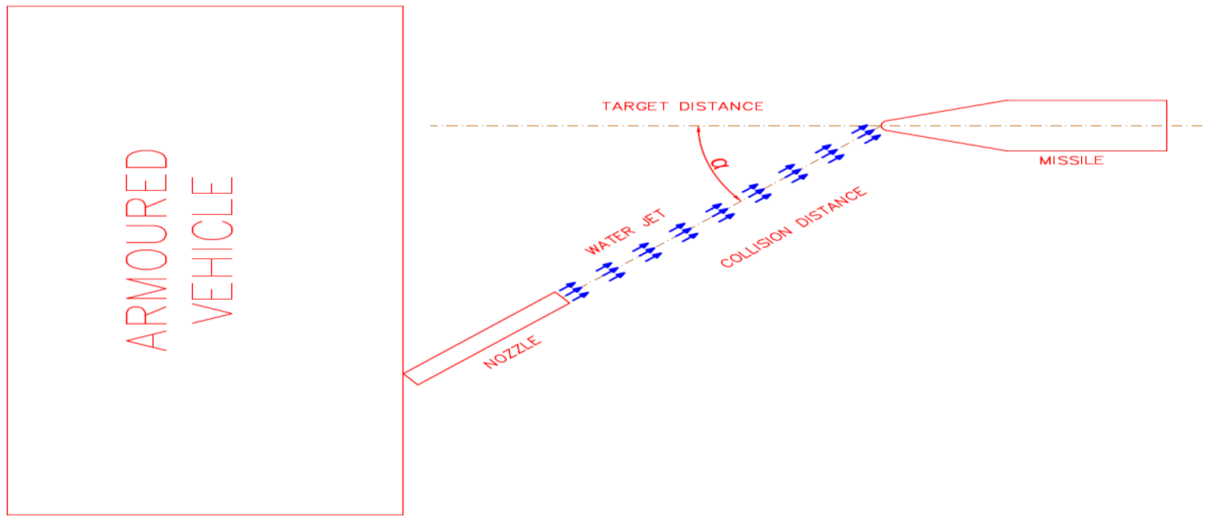

Figure 4.26. WJ and missile interaction for different AoC

5. CONCLUSIONS

The aim of this study is to examine the deformation progress and change in motion of an anti-tank missile which is subjected to a high-pressure water jet flow. In the literature there are many studies investigating water jets as an industrial tool for cutting alloyed metals and steels, rain drop erosion in high-speed flight zone, soil erosion due to farming and watering, mining, suppressing riots with water cannons, no study was encountered in which the water jet was used as an active protection system.

High pressure water jet characteristics are revealed due to;

- Different nozzle diameters
- Different collision distance of water jet and missile
- Different jet velocities

In this thesis "Smooth Particle Hydradynamics - SPH" method of ANSYS Ls-Dyna programme was used.

In the numerical study the problem has been defined, model geometry is drawn and the necessary calculations have been made on the boundary conditions.

Because lack of experimental results for the study, the numerical model cannot be directly validated with experimental studies. On the other water cannon force and pressure experiments' results are iterated to approach a meaningful numeric value.

According to the results of the study due to variable collision distance,

- Nozzle diameter: 2mm. Water jet velocity: 150 m/s. Collision distance is increased from 200 mm to 300 mm. Resultant momentum stayed constant with a value of 0.017 kgm/s. The change in impuls is 0.00884 to 0.01421 MPa.ms respectively.
- Nozzle diameter: 4 mm. Water jet velocity: 500 m/s. Collision distance is increased from 300 mm to 400- and 600-mm. Resultant momentum increased from 0.213 to 0.278 kgm/s in the coherent zone up to 400mm. Out of this region slightly decreased from 0.278 to 0.267 kgm/s. Impuls increased from 7.14 MPa.ms to 11.33 MPa.ms in the coherent zone and decreased to 7.44 MPa.ms at 600 mm distance.

- Nozzle diameter: 6 mm. Water jet velocity: 500 m/s. Collision distance are 300- and 600-mm. Resultant momentum increased from 0.197 to 0.474 kgm/s with increasing distance. Impuls changed directly proportional to distance from 5.38 to 7.198 MPa.ms
- Nozzle diameter: 10 mm. Water jet velocity: 500 m/s. Collision distance are 600- and 1000-mm. Resultant momentum decreased from 0.798 to 0.77 kgm/s with increasing distance. Impuls changed inverse proportional to distance from 6.14 to 4.4494 MPa.ms
- Collision distance between 200-1000 mm. Nozzle diameter: 6 mm. Resultant momentum varied from 0.064 to 0.474 kgm/s with an increment ratio of 86.5%. Impuls value's range is 4.45 to 7.19 MPa.ms. 38.07 % increase was seen. In this range for 150 m/s WJ velocity Resultant momentum and impuls values increased 86.5 % and 99.6% respectively.

Variable Velocity,

- Nozzle diameter: 2 mm. Collision distance: 300 mm. Water Jet velocity are 150 and 500 m/s. Resultant momentum stayed constant at 0.017 kgm/s. Impuls value can not be read for 500 m/s velocity and is 0.014 MPa.ms for 150 m/s.
- Nozzle diameter: 4 mm. Collision distance: 300 mm. Water Jet velocity are 150 and 500 m/s. Resultant momentum decreased from 0.229 to 0.213 kgm/s with increasing values of velocity. Impuls value decreased from 7.223 to 7.1398 MPa.ms inverse proportional to velocity.
- Nozzle diameter: 6 mm. Collision distance: 300 mm. Water Jet velocity are 150 and 500 m/s. Resultant momentum increased from 0.064 to 0.197 kg.m/s with increasing velocity. Impuls value increased from 4.4584 to 5.38 MPa.ms directly proportional with velocity.
- Nozzle diameter: 10 mm. Collision distance: 300 mm. Water Jet velocity are 150 and 500 m/s. Resultant momentum increased from 0.327 to 0.798 kg.m/s with increasing velocity. Impuls value increased from 2.54 to 6.14 MPa.ms directly proportional with velocity.
- Velocity distribution between 150 – 500 m/s. Nozzle diameter: 4 mm. Resultant momentum increased from 0.229 to 0.267 kgm/s with a 14.3 % ratio. Impuls value increased 3.01 % from 7.22 to 7.44 MPa.ms. When collision distance is 300 mm resultant momentum and impuls values changed negatively. From 0.229 to 0.213 kgm/s and 7.22 to 7.13 MPa.ms. Decrease rates are 7.51 % and 1.17%.

Variable Nozzle Diameter,

- Water jet velocity: 150 m/s and Collision distance is 300 mm. Maximum resultant momentum and impuls values are observed for a nozzle diameter of 4 mm 0.229 kgm/s and 7.223 MPa.ms respectively. 2 mm nozzle gave the smallest results of 0.017 kg.m/s and 0.014 MPa.ms. 6 mm nozzle; unlike the expected results gave the intermediate values of 0.064 kg.m/s and 4.45 MPa.ms
- Water jet velocity: 500 m/s and Collision distance is 300 mm. Maximum resultant momentum and impuls values are observed for a nozzle diameter of 4 mm 0.213 kgm/s and 7.139 MPa.ms respectively. 2 mm nozzle gave the smallest results of 0.017 kg.m/s. Impuls values can not be determined. 6 mm nozzle's results are 0.197 kg.m/s and 5.3828 MPa.ms
- Water jet velocity: 500 m/s and Collision distance is 600 mm. Results are evaluated for 4,6 and 10 mm nozzles. Resultant momentum values are 0.267, 0.474 and 0.798 kg.m/s respectively. Impuls is 7.44 – 7.19 and 6.14 MPa.ms for 4-6- and 10-mm nozzles.
- Nozzle diameter is 2,4,6 and 10 mm. WJ velocity 150 m/s. Resultant momentum increased from 0.017 to 0.327 kgm/s with a ratio of 94.8 % and impuls increased from 0.0088 to 2.54 MPa.ms. Increment ratio is 99.65%. When collision distance is 300 mm, resultant momentum increased from 0.017 to 0.064 kgm/s with a ratio of 73.44 % and impuls increased from 0.01421 to 4.45 MPa.ms. Increment ratio is 99.68%.

Missile Deactivating and Diverting

- According to APS blast calculations impuls value of 0.36 MPa.ms, momentum value of 3.2 kgm/s and pressure value of 13.76 MPa is enough to detonate the missile. Nozzles having diameter over 4 mm generate 2.54 MPa.ms impuls and 40.65 MPa pressure values which will deactivate the missile.
- Water jets capacity to divert missile over 4 mm nozzle capacity is evaluated for 30^0-45^0 and 60^0 interaction angles. 2,6-38,26 mm, 2.47-35.09 mm, and 1.49-20.51 mm deflection was seen respectively.

6. RECOMMENDATIONS

The results of this study may be a source for industrial applications such as high-pressure water jet cutting, mining, cleaning and for military purposes like discarding ammunitions and as a counter measure for threats, protecting armoured land vehicles.

In the future studies related to this thesis topic:

- The collision distance may be increased, and calculations can be carried on much longer safe distances.
- Different nozzle geometry with a different spray characteristic and diameter can be studied.
- Work can be carried on with different fluids such as non-newtonian, abrasive additive and nanofluid jets.
- Ambient temperature, density and media can be varied to investigate different solid/fluid interaction.
- Variation of water jet behaviour due to temperature can be examined.
- Missile types which will have different mass, momentum and explosive charge values can be studied.
- Water jet effect on missile can be investigated for different interaction angles to understand the deviation proses after contact.
- Differences between swirling jets and impinging jets effects on missile can be research concern.
- Application of water jets to different armoured land vehicles can be studied to understand vehicle capacity.
- Electrical saltwater cannon may be considered as a protection system.

.

REFERENCES

Jacinto, A., Ambrosini, R. and Danesi, R., 2001. Experimental and computational analysis of plates under air blast loading. International Journal of Impact Engineering, 25(10), pp.927-947.

Li, C. and Hong, W. (2017). A study of aerodynamic characteristics of an anti-tank missile. SAHSS-2017, LEBCSR-17, LERIS-2017, Jan. 31-Feb. 1, 2017 Bali (Indonesia). doi:10.17758/eirai.f0217101.

Tai, C. H., Teng, J. T., Lo, S. W. and Liu, C. W. (2007). A numerical study in the interaction of blast wave with a wheeled armoured vehicle. International Journal of Vehicle Design, 45(1/2), 242. https://doi.org/10.1504/ijvd.2007.013680.

Guha, A., Barron, R. M. and Balachandar, R. (2011). An experimental and numerical study of water jet cleaning process. Journal of Materials Processing Technology, 211(4), 610–618. https://doi.org/10.1016/j.jmatprotec.2010.11.017.

Trettel, B. and Ezekoye, O. A. (2015). Theoretical range and trajectory of a water jet. Volume 7A: Fluids Engineering Systems and Technologies. doi:10.1115/imece2015-52103.

Adler, W. F. (1995). Waterdrop impact modeling. Wear, 186-187, 341-351. doi:10.1016/0043-1648(95)07176-8.

Bowden, F. P. and Brunton, J. H. (1958). Damage to solids by liquid impact at supersonic speeds. Nature, 181(4613), 873-875. doi:10.1038/181873a0.

Hashish, M. and DuPlessis, M. P. (1978). Theoretical and experimental investigation of continuous jet penetration of solids. Journal of Engineering for Industry, 100(1), 88-94. doi:10.1115/1.3439351.

Heymann, F. J. (1969). High-speed impact between a liquid drop and a solid surface. Journal of Applied Physics, 40(13), 5113-5122. doi:10.1063/1.1657361.

Lee, M. K., Kim, W. W., Rhee, C. K., & Lee, W. J. (1999). Liquid impact erosion mechanism and theoretical impact stress analysis in tin-coated steam turbine blade materials. Metallurgical and Materials Transactions A, 30(4), 961-968. doi:10.1007/s11661-999-0149-y.

Yang, Y., Liou, W., Sheng, J., Gorsich, D. and Arepally, S. (2011). Shock wave impact simulations using fluid/structure/dynamics interactions. SAE Technical Paper Series. doi:10.4271/2011-01-0258.

Baykara, T., Günay, V. and Demirural, A. (2021). Structural evolution And Microstructural features of the hydrodynamically Penetrating Copper jet of a shaped charge. Journal of Materials Engineering and Performance, 30(3), 1862-1871. doi:10.1007/s11665-021-05514-9.

Rochester, M. C. (1978). The impact of a liquid drop with a solid surface and the effects of the properties of the liquid on the erosion of solids (Unpublished master's thesis). University of Plymouth. Retrieved from http://hdl.handle.net/10026.1/1939.

Bailey, J. L., Farley, J. P., Williams, F. W., Lindsay, M. S., and Schwer, D. A. (2006). Blast mitigation using water mist. doi:10.21236/ada443885.

Tatekura, Y., Watanabe, M., Kobayashi, K., and Sanada, T. (2018). Pressure generated at the instant of impact between a liquid droplet and solid surface. Royal Society Open Science, 5(12), 181101. doi:10.1098/rsos.181101.

Sibille, R., & Tasset, N. (2020). Characterization of the erosion resistance of coatings for aerospace and windmill applications. Retrieved April 11, 2021, from http://hdl.handle.net/2078.1/thesis:26535.

Gurney, R. W. (1943). The initial velocities of fragments from bombs, shell, grenades. doi:10.21236/ada289704.

Ohlsson, L. (1995). The theory and practice of abrasive water jet cutting (Doctoral dissertation, Luleå, 1995). Luleå: Univ.

Leach, S. J., Walker, G. L., Smith, A. V., Farmer, I. W., and Taylor, G. (1966). Some Aspects of Rock Cutting by High Speed Water Jets [and Discussion]. Philosophical Transactions of the Royal Society of London. Series A, Mathematical and Physical Sciences, 260(1110), 295–310. Retrieved from http://www.jstor.org/stable/73558.

Chant, C. (2013). A compendium of armaments and military hardware. Retrieved April 11, 2021, from https://www.amazon.com/Compendium-Armaments-Military-Hardware-Routledge/dp/0415710723.

Meyer, T. J. (1998). Active Protective Systems: Impregnable Armor or Simply Enhanced Survivability? ARMOR — May-June, 7–11. https://fas.org/man/dod-101/sys/land/docs/3aps98.pdf.

WARDJet. (n.d.). Waterjet University - Pumps. Retrieved April 11, 2021, from https://wardjet.com/waterjet/university/pumps.

Warhead. (2021). Retrieved April 11, 2021, from https://en.wikipedia.org/wiki/Warhead.

Feickert, A. (2017, March 10). Army and Marine Corps active protection System (APS) Efforts. Retrieved April 11, 2021, from https://digital.library.unt.edu/ark:/67531/metadc958725/.

Plunger pump. (2020). Retrieved from Wikipedia website: https://en.wkipedia.org/wiki/Plunger_pump.

The medical implications of vehicle-mounted water cannon with special reference to the Ziegler Wasserwerfer 9000 (WaWe 9) system (pp. 1-106, Rep.). (2013). Salisbury, England: DSTL Biomedical Sciences.

Medical implications of the use of vehicle mounted water cannon (pp. 1-96, Issue brief No. 2). (2004). Salisbury, England: DSTL.

Wilkinson, J. and Watt, D. (2006). Munitions Safety Information Analysis Center Centre d'information et d'analyse sur la sécurité des munitions REVIEW OF DEMILITARISATION AND DISPOSAL TECHNIQUES FOR MUNITIONS AND RELATED MATERIALS. Retrieved from website: http://rasrinitiative.org/pdfs/MSIAC-2006.pdf.

Gauert, C., Van der Westhuizen, W., Claasen, J., Viljoen, S., & Grobler, J. (2013). A progress report on ultra-high-pressure waterjet cutting underground: The future of narrow reef gold and PGE mining. J. South. Afr.Inst. Min. Metall. 2013, 113, 441–448.

Water Jet CuttingA Technology on the Rise [Brochure]. (2010). Retrieved from https://www.kmt-waterjet.pl/PDF/KMT_technology description_ENG_101019.pdf.

Hashish, M. (2009). Special AWJ Nozzles. Paper presented at American WJTA Conference and Expo, Houston, Texas. Retrieved from http://www.wjta.org/images/wjta/Proceedings/Papers/2009/I3 Hashish.pdf.

Jonsson, R. (2007). Characterisation and validation of a pulsating jet erosion test (Dissertation). Retrieved from http://urn.kb.se/resolve?urn=urn:nbn:se:ltu:diva-48676.

Jenzen-Jones, N. R., Ferguson, J., and Williams, A. G. (2018). Weapons Identification: Light Weapons and their Ammunition (N. R. Jenzen-Jones, and M. Schroeder, Eds.). In An Introductory Guide to the Identification of Small Arms, Light Weapons, and Associated Ammunition (pp. 167-230). Geneva, Switzerland: Small Arms Survey.

Brunton, J. H. and Rochester, M. C. (1979) Erosion of solid surfaces by the impact of liquid drops. In: Treatise on Materials Science and Technology, Volume 16, pp.185-248.

Schwartzentruber, J., Narayanan, C., Liu, H. T., & Papini, M. (2016). Optimized abrasive waterjet nozzle design using genetic algorithms. 23rd International Conference on Water Jetting. Seattle: BHR Group.

Yevdokimov, B.I. (1967) Antitank rocket missiles [Brochure]. Foreign technology division. Air force systems command Moscow, Russia.

Engel, O. G. (1955). Waterdrop collisions with solid surfaces. Journal of Research of the National Bureau of Standards, 54(5), 281. https://doi.org/10.6028/jres.054.033.

Kmeč, J., Hreha, P., Kuběna, V., Knapčíková, L., Mačej, T., Hlaváček, P., … Cumin, J. (2010). Disposal of discarded munitions by liquid stream. Tehnički Vjesnik, 17(3), 383–388. Retrieved from https://hrcak.srce.hr/59654.

Rajaratnam, N., Rizvi, S. A. H., Steffler, P. M., & Smy, P. R. (1994). An experimental study of very high velocity circular water jets in air. Journal of Hydraulic Research, 32(3), 461–470. https://doi.org/10.1080/00221689409498746.

Miller, P. (2018) A Retrospective Study on the Safety of Waterjet (WJ) and Abrasive Waterjet (AWJ) Processing of High Explosive Ordnance. Retrieved from https://ndiastorage.blob.core.usgovcloudapi.net/ndia/2018/intexpsafety/MillerPaulPosterPaper.pdf.

Moylan, B., Landrum, B., & Russell, G. (2013). Investigation of the Physical Phenomena Associated with Rain Impacts on Supersonic and Hypersonic Flight Vehicles. Procedia Engineering, 58, 223–231. https://doi.org/10.1016/j.proeng.2013.05.026.

ASM Material Data Sheet. (n.d.). Retrieved from asm.matweb.com website: http://asm.matweb.com/search/SpecificMaterial.asp?bassnum=MA2219T81.

Medan, N. (2016). Evaluation of Nozzle Coefficients for Water Jet Used in Sewer Cleaning. Hidraulica. 14-20.

Lopatnikov, S. L., Gillespie, J. W., Morand, C., Lumpkin, R., & Dignam, J. (2012). The New Test Method for High Velocity Water Jet Impact. Experimental Mechanics, 52(9), 1475–1481. https://doi.org/10.1007/s11340-012-9608-2.

Vasilis, K. & Solomos, G. (2013) Calculation of Blast Loads for Application to Structural Components. European Commission Joint Research Centre.

Luo, H., Ma, Y., & Hu, X. (2015). Analysis on Fragmentation Injury of Glare Stun Grenade. Proceedings of the First International Conference on Information Sciences, Machinery, Materials and Energy. https://doi.org/10.2991/icismme-15.2015.395.

Wey, P., Fleck, V. & Chanteret, P.Y. (2001). Analysis of Active Protection Systems - When ATHENA Meets ARENA.

Janzon, B., Backofen, J., Brown, R.E., Cayzac, R., Diederen, A., Giraud, M., Held, M., Horst, A., & Thoma, K. (2007). The Future of Warheads, Armour and Ballistics. 23rd International Symposium on Ballistics ,Tarragona, Spain , Vol. 1 pp. 3– 27.

Song, C., Yao, L., & Xiao, Z. (2018). Data-Fusion-Based Detect Equipment of Tank Initiative Defense System. MATEC Web of Conferences, 228, 01008. https://doi.org/10.1051/matecconf/201822801008.

Mohamed, M. A. (2004). Waterjet cutting up to 900 mpa (PhD. thesis, Hannover, University, Diss, 2004). S.l.: S.n. doi:https://doi.org/10.15488/6410.

Texas Instruments. (2011). Electronic Fuzing [Brochure]. Dallas, Texas: Author. Retrieved December 5, 2020, from https://www.ti.com/lit/an/snoa217/snoa217.pdf?ts=1618268018483&ref_url=https%253A%252F%252Fwww.google.com%252F.

Frost, D. L., Ornthanalai, C., Zarei, Z., Tanguay, V., and Zhang, F. (2007). Particle momentum effects from the detonation of heterogeneous explosives. Journal of Applied Physics, 101(11), 113529. doi:10.1063/1.2743912.

Fleeman, E. L. (2001). Tactical missile design. Reston, Va: American Institute Of Aeronautics And Astronautics.

Livermore Software Technology Corporation (2019) LS-DYNA® Theory Manual. Livermore, CA: Author.

CURRICULUM VITAE